Control Design for a Microgrid in Normal and Resiliency Modes of a Distribution System

Genesis Barbie Alvarez

Thesis submitted to the Faculty of the
Virginia Polytechnic Institute and State University in partial fulfillment of the requirements for the degree of

Master of Science

in

Electrical Engineering

Chen-Ching Liu, Chair

Jamie De La Reelopez

Virgilio A Centeno

September 5th, 2019

Blacksburg, Virginia

Keywords: Distributed Energy Resources, Microgrid, Volt/Var Control, Resiliency Source and

Control Design for a Microgrid in Normal and Resiliency Modes of a Distribution System

Genesis Barbie Alvarez

(ABSTRACT)

As inverter-based distributed energy resources (DERs) such as photovoltaic (PV) and battery energy storage system (BESS) penetrate within the distribution system. New challenges regarding how to utilize these devices to improve power quality arises. Before, PV systems were required to disconnect from the grid during a large disturbance, but now smart inverters are required to have dynamically controlled functions that allows them to remain connected to the grid. Monitoring power flow at the point of common coupling is one of the many functions the controller should perform. Smart inverters can inject active power to pick up critical load or inject reactive power to regulate voltage within the electric grid. In this context, this thesis focuses on a high level and local control design that incorporates DERs. Different controllers are implemented to stabilize the microgrid in an Islanding and resiliency mode. The microgrid can be used as a resiliency source when the distribution is unavailable. An average model in the D-Q frame is calculated to analyze the inherent dynamics of the current controller for the point of common coupling (PCC). The space vector approach is applied to design the voltage and frequency controller. Secondly, using inverters for Volt/VAR control (VVC) can provide a faster response for voltage regulation than traditional voltage regulation devices. Another objective of this research is to demonstrate how smart inverters and capacitor banks in the system can be used to eliminate the voltage deviation. A mixed-integer quadratic problem (MIQP) is formulated to determine the amount of reactive power that should be injected or absorbed at the appropriate nodes by inverter. The Big M method is used to address the nonconvex problem. This contribution can be used by distribution operators to minimize the voltage deviation in the system.

Control Design for a Microgrid in Normal and Resiliency Mode of a Distribution System

Genesis Barbie Alvarez

(GENERAL AUDIENCE ABSTRACT)

Reliable power supply from the electric grid is an essential part of modern life. This critical infrastructure can be vulnerable to cascading failures or natural disasters. A solution to improve power systems resilience can be through microgrids. A microgrid is a small network of interconnected loads and distributed energy resources (DERs) such as microturbines, wind power, solar power, or traditional internal combustion engines. A microgrid can operate being connected or disconnected from the grid. This research emphases on the potentially use of a Microgrid as a resiliency source during grid restoration to pick up critical load. In this research, ccontrollers are designed to pick up critical loads (i.e hospitals, street lights and military bases) from the distribution system in case the electric grid is unavailable. This case study includes the design of a Microgrid and it is being tested for its feasibility in an actual integration with the electric grid. Once the grid is restored the synchronization between the microgrid and electric must be conducted. Synchronization is a crucial task. An abnormal synchronization can cause a disturbance in the system, damage equipment, and overall lead to additional system outages. This thesis develops various controllers to conduct proper synchronization. Interconnecting inverter-based distributed energy resources (DERs) such as photovoltaic and battery storage within the distribution system can use the electronic devices to improve power quality. This research focuses on using these devices to improve the voltage profile within the distribution system and the frequency within the Microgrid.

Dedication

To my parents, Barbaro Alvarez and Luz Lopez, and my grandmother Conceptíon Lopez

Acknowledgments

I am grateful to my lord and saviour for blessing me with the opportunity of attending Virginia Tech and the experience I had here.

This research project was generously sponsored by Dominion Virginia Power. I would like to thank Kyle Thomas, Joseph Petti, Dr. Hung Ming Chou, Dr. Ren Liu and Christopher Mertz for their mentorship and numerous conversations on this research that helped form part of this thesis.

I am very grateful towards my advisor Dr. Chen-Ching Liu for his guidance, support and patience. Without his advice and inspiration, this work would not be possible. I would like to express my appreciation to Dr. Jaime De La Ree and Dr. Virgilio Centeno for being on my committee and for giving me guidance and encouragement academically and personally. Apart from my committee members I would like to thank professor Vassilis Kekatos, Craig Woolsey and Rolando Burgos for deepening my knowledge in power system distribution, control theory and power electronics.

I have gained many cherished memories within Virginia Tech that I will never forget. Most of them being from my fellow colleagues Nitasha, Pratigya, Anaga, Yousef, IK and Shuchismita. Many admirable students have offered me support within these past two years, Manish and Mana with their discussions on optimization, Tapas with his mentorship, Ye with her advice in debugging software, Hua, Rebecca and Sina with their discussions on power electronic devices. I have also been fortunate to had made incredible friends through New Horizons and the Graduate Society of Hispanic Professionals Engineers (GradSHPE) chapter: Adrian, Anthony, John, Mark, Katrina and Katherine. I would like to thank the two ladies who I would share late night conversations, continuous adventures and the many laughs we encounter together, to my two roommates, Grace and Sherin.

I came to know about the lifestyle, education and the people in Virginia Tech by Ivette, she was my mentor during my undergraduate years and I am truly grateful she encouraged me to apply. I would like to mention my friend Leticia who I have known since my childhood and who has always motivated and been there for me. Finally, I am truly thankful to my parents and siblings, Susan, Barbaro and Eric for pushing me to achieve my greatest potential.

Table of Contents

List of Figures

viii

List of Tables

Chapter 1

Introduction

This chapter explains the motivation behind this research topic and the general concept of the MG and its importance. Also, a detailed objective of this research is mentioned. Finally, the layout of this thesis is explained for each chapter.

1.1 Motivation

Historically, natural disasters have been the root cause of severe power outages around the world. As the distribution grid remains vulnerable to natural disasters it is important to focus on grid resilience, which is defined as the grid's capability to continuously function and maintain the critical load during an extreme event such as earthquakes, floods, tornados and hurricanes. Recently, on September 17th, 2018 hurricane Maria impacted 1.5 million of people and is it is known as the largest blackout in the United States [1]. It took 11 months for Puerto Rico to restore its electric power. Due to this catastrophic event patients in hospitals were unable to use essential medical equipment. During these disastrous events, critical infrastructures (i.e. emergency responders, water stations, street lights, hospitals and military bases) can be considered as a critical load. It is significant to restore and provide power to critical loads. National Laboratories such as the National Laboratory of Renewable Energy (NREL), Pacific Northwest National Laboratory (PNNL), Oak Ridge National Laboratory (ORNL) and Sandia National Laboratories have evaluated and analyze the power generation opportunity such as a Microgrid (MG) to improve the resiliency in the distribution system of Puerto Rico. ORNL has worked on a project that predicts the electric grids dynamic behaviour that is impacted by a natural disaster.

The need for Distributed Generations (DGs) is increasing because of the potential it must alleviate the burden to the electric grid by supplying power to critical loads. However, the integration between the two can cause issues if it is not properly managed. Recently there has been a focus on projects that develop and implement Microgrids by the U.S. Department of Energy (DOE), Department of Defence (DOD) and power utilities companies [2]. The first Microgrid (MG) concept was introduced by Thomas Edison when he opened Pearl Street Station in New York City. This system only provided power to a few blocks due to the direct current network limitation. The load demand since then has increased and large scale alterative current transmission lines interconnected multiply utilities. The Consortium for Electric Reliability Technology Solutions (CERTS) conducts research since 1999 on ways to enhance the reliability of the electric grid [3]. Since then the popularity of MGs has increased immensely; Navigant Reach identified 1,869 MG projects in the world, representing 20.7 GW, in 2017 [4]. With the new excessive integrated distributed generation, a challenge in system operation and control is introduced. Utilities have been addressing these problems by using the inverter based distributed resources for power flow and voltage and frequency control. Standards and regulations such as the IEEE Standard 1547[5] and the California Public Utility Commission Rule 21[6] have been in place to make sure that smart inverters can conduct functions. For example, the distributed energy resources (DERs) should provide voltage regulation capabilities such as:

- Constant power factor mode

- Voltage-reactive power mode
- Active power-reactive mode
- Constant reactive power mode

Utilities are now investigating the control methodology implemented within a MG to maintain the system performance regarding the voltage and frequency.

1.2 Objective

Dominion Energy is an electric utility company that produces and transports energy of approximately 26,000 megawatts in the United States. Dominion Energy is expanding a storage yard into a campus, which is the opportune time to develop a MG. The main goal for this MG is to be able to island and provide power to critical loads during an outage or severe weather condition. This MG project is part of the Grid Transformation & Security Act, which describes the first three years ("Phase I") of a proposed 10-year program that will enhance the reliability, resiliency and security of the electric distribution grid, improve service for customers, and provide them with more options for communications and control as well as tools for managing their energy use [7]. As the company becomes familiarized with the MGs functionality, it will be possible to provide MGs as a service for hospitals, university campuses and military bases. The objective of this research is to design and model the MG, including the diesel generator, PV arrays, load and batteries, to analyze the feasibility of the MG by conducting various cases studies.

1.2 Microgrid Concept

The U.S. Department of Energy defines a MG as "a group of interconnected loads and distributed energy resources within clearly defined electrical boundaries that acts as a single controllable entity with respect to the grid. A microgrid can connect and disconnect from the grid to enable it to operate in both grid-connected or island-mode" [6]. Overall the MG is a controllable system that can be operated in either disconnected or connected to the grid. Unlike conventional back up generation a MG can have a combination of Disturbed Generations (DGs). The distributed generations (DGs) in a MG can be microturbines, biomass, wind power, geothermal power, fuel cells, solar power, or traditional internal combustion engines. Due to the low inertia in these distributed energy resources, power electronic equipment needs to be interfaced to synchronized properly to the electric grid. Some advantages that a microgrid has is that they produce clean energy, reduce peak loads, provide ancillary services to the grid and can pick up and serve critical loads in the local distribution network when the utility grid is not available. It is important for utilities to do research in this area because MGs will be a contributing factor to improve the grids' resiliency. Having a MG that is self-sustained will control the increasing penetration of DG and enhance the resiliency of the distributed system.

1.3 Microgrid in a Restoration Mode

In the conventional power system several functions must be performed before establishing system restoration [7]:

- Reactive power balancing
- Load and generation balance
- Switching transient voltages
- Local load shedding
- Under-frequency and switched capacitor relays
- Cold load pickup

- Sequencing of generating units start up

Since the MG is much smaller than a utility grid, the restoration process should be much quicker. Similar to the load management function within the electric grid where the utility compensates the customers for shutting off their load to regulate frequency and voltage. A MG should also have a power management controller (PMC) that recognizes a power loss in the grid and the microgrid switches to an emergency mode and conducts load shedding for non-critical. Due to the battery storage capacity and the unpredictable state of charge the battery storage may be in it is better to shed load to conserve the energy in the BSSE and prioritize the critical load not only in the MG but also in the local distribution system. In an islanded mode (autonomous mode) the power management system in reference [8] uses the inverter-based DG to rapidly control the real and reactive power the diesel generator is used during steady-state power management, both based on locally measured signals making the controllers operate based on local information.

During the absence of the power utility a MG can act as the resiliency power source to serve critical loads. Methods have been researched that uses the MG to restore critical load. A linear integer problem that maximizes the number of critical loads that are restored based on priority and minimizes the quantity of non-critical load is proposed in [9]. To reduce restoration time a procedure was analysed in [10] by implementing a microgrid central controller (MGCC) that transmits information such as switching sequences and set points to the local controller during the black start process. A central controller not only can be used for restoration purposes but also for a steady-state analysis to conduct voltage regulation, power flow analysis and scheduling strategies to minimize net cost as per [11-14].

1.4 Contributions

This thesis proposes a MG design for Dominion Energy that is capable to function in islanded mode, grid-connected mode and in restoration mode. Having a MG within their system will allow them to pick up a critical load from the nearby distribution network during a restoration mode. In this research the ability to pick up a critical load with the Dominion Energy MG proposal is explored by implementing a Linear Quadratic Regulator (LQR) and multiply Proportional-Integral (PI) controllers.

A central controller is also designed to improve power quality within the distribution system, particularly the voltage by using smart inverters interconnected by the DERs and the MG. Using inverters for Volt/VAR control (VVC) can provide a faster response for voltage regulation than traditional voltage regulation devices, such as transformer load tap changers and voltage regulators. The primary objective of chapter 5 is to demonstrate that smart inverters can be used to eliminate the voltage deviation by solving a mixed-integer quadratic program to determine the amount of reactive power that should be injected or absorbed at the appropriate nodes. The proposed method incorporates capacitor banks connected to the network and determines whether use the nearby inverter or to turn on or off the capacitor bank for voltage regulation. These processes will be demonstrated in several cases that are focused on mitigating voltage-dips and swells.

1.5 Thesis Outline

This thesis is organized into five chapters including the current one that introduces the overall concept of the MG and mentions the motivation and objective for this research the rest chapters are organized as follows.

Chapter 2 mentions the background theory used within this thesis including diagrams and equations to deliver a better understanding to the general audience,

Chapter 3 describes the MG design procedure for the roof mounted solar, ground mounted and the solar canopies. This chapter models the MG into an existing campus expansion plan. To validate the designed MG, a model of the MG is constructed in a Real Time Simulator Computer Aided Design (RSCAD) and is simulated using a Real Time Digital Simulator (RTDS). Two case studies are performed, including the synchronization and the battery frequency regulation assistance. The simulation results show the feasibility of the designed MG.

In Chapter 4 a current and voltage controller is designed to operate while the transmission side is in restoration mode. The MG is used as a resiliency source to pick up the critical load within the local distribution network. The current controller uses a linear quadratic regulator to obtain the optimal state feedback gain for the system and it uses a proportional-integral (PI) controller that receives the feedback signals. A PI is also used to design the voltage controller and the design procedure is included within this chapter. A case study is done in SIMULINK/MATLAB modelling the MG designed in chapter 3 and the critical load is picked up from the distribution system by the Battery Energy Storage System (BESS) and the diesel generator within the MG.

Chapter 5 addresses how using inverters for Volt/VAR control (VVC) can provide a faster response for voltage regulation than traditional voltage regulation devices, such as transformer load tap changers and voltage regulators. The primary objective of this chapter is to demonstrate how smart inverters within a DG or MG can be used to eliminate the voltage deviation within the distribution system by solving a mixed-integer quadratic program to determine the amount of reactive power that should be injected or absorbed at the appropriate nodes. The proposed method incorporates capacitor banks connected to the network and determines whether to turn on or off the capacitor bank for voltage regulation. These processes will be demonstrated in several cases that are focused on mitigating voltage-dips and swells.

Chapter 6 provides a summary of the thesis and includes possible extension of this research.

Chapter 2

Background

This chapter explains the basic knowledge to study the system presented and the type of control methodology applied in this research. This is essential for the controller design process.

2.1 Dynamic Average Model for a Three-Phase System

When establishing the control design for the inverter during a continuous time frame, developing a dynamic average model will increase the speed of computation in comparison to the detailed switching model. The average model [15] has been developed by linearizing the dynamic system and applying the moving average operator to the switching model. The switch duty cycle d is the moving average of the switching function $s(t)$.

$$\bar{x}(t) = \frac{1}{T}\int_{t-T}^{t} x(\tau)d\tau$$

Generally, the three-phase system is represented by the abc- frame however a time variant three-phase variable can also be represented by the $\alpha\beta$-frame and the dq-frame by applying the Clarke and Park transformation [16]. The direct-quadrature-zero (dq) transformation will be applied to the phase-neutral variables within this thesis. The average model is in the rotating dq -coordinates.

$$T_n = T_{dq0\backslash abc} = \sqrt{\frac{2}{3}}\begin{bmatrix} cos(\omega t) & cos(\omega t - \frac{2\pi}{3}) & cos(\omega t + \frac{2}{3}\pi) \\ -sin(\omega t) & -sin(\omega t - \frac{2\pi}{3}) & -sin(\omega t + \frac{2\pi}{3}) \\ \frac{1}{\sqrt{2}} & \frac{1}{\sqrt{2}} & \frac{1}{\sqrt{2}} \end{bmatrix} \quad (2.1a)$$

To calculate the abc variables from the $dq0$ the inverse transformation is:

$$T_n^{-1} = T_{abc\backslash dq0} = \sqrt{\frac{2}{3}}\begin{bmatrix} cos(\omega t) & -sin(\omega t) & \frac{1}{\sqrt{2}} \\ cos(\omega t - \frac{2\pi}{3}) & -sin(\omega t - \frac{2\pi}{3}) & \frac{1}{\sqrt{2}} \\ cos(\omega t + \frac{2}{3}\pi) & -sin(\omega t + \frac{2\pi}{3}) & \frac{1}{\sqrt{2}} \end{bmatrix} \quad (2.1b)$$

The differential equations can be obtained by conducting a circuit analysis and utilizing Kirchhoff's Voltage and Current laws from the DC bus to the grid. The angle used in the transformation equations in (2.1a-2.1b) can be found by using a phase-locked loop.

2.2 Phase Locked Loop

A phase locked loop (PLL) consists of a phase detector, loop filter and a voltage -controlled oscillator (VCO). The phase detector generates an output signal proportional to the phase difference between the two input signals. The loop filter is a low pass filter which filters the high frequency from the phase detector output. The voltage control oscillator determines the oscillating frequency based on the input voltage. There are different types of PLL [17-18]. A commonly used PLL is the synchronous reference frame (SRF) PLL as demonstrated in Figure 2.1. The symbol ω_0 is the desired angular frequency at the steady state and PI is a proportional -integral controller.

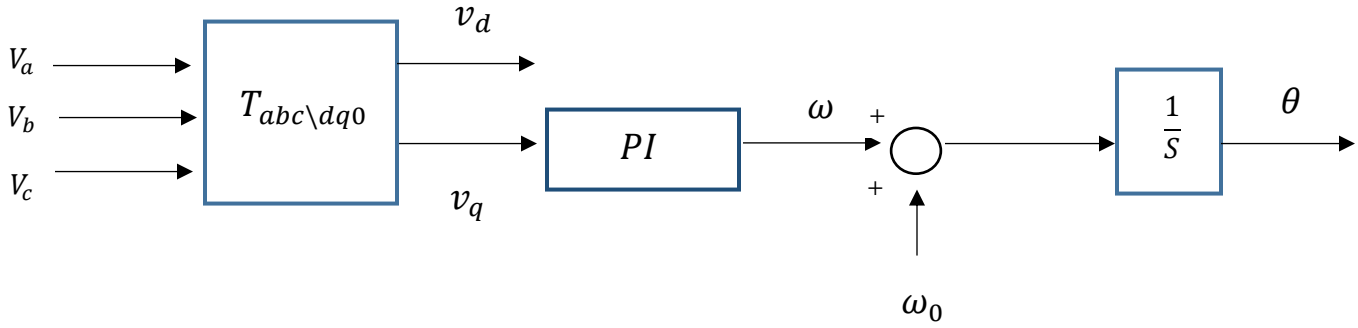

Figure 2.1 Synchronous Reference Frame Phase Locked Loop (PLL)

2.3 Linear Quadratic Regulator

The Linear Quadratic Regulator (LQR) is an optimal control method used to compute the state feedback control gain matrix. An LQR can be used for either a time varying or a time-invariant system. The LQR control problem is defined as finding an optimal control law $u^*(t) := -Kx(t)$ for the linear system (2.2aa) which minimizes the quadratic cost function (2.2b).

$$\dot{x} = A(t)x + B(t)u, \quad x(t_0) = x_0 \tag{2.2a}$$

$$J = \int_0^\infty [x(\tau)^T Q(\tau)x(\tau) + u(\tau)^T R(\tau)u(\tau)]d\tau \tag{2.2b}$$

Q and R are designed to minimize the performance index (J). Q is the state penalty matrix, and it should be positive semi-definite. R is a control penalty matrix that should be positive definite. If the system is controllable and observable there exists a constant control law that makes the closed-loop system asymptotically stable [19]. A linear system is controllable if and only if

$$rank\ [B|AB|\ldots|A^{n-1}B] = n$$

where n is the number of state variables in the system. Similarly, a system is ed observable if and only if

$$rank\begin{bmatrix} C \\ CA \\ \vdots \\ CA^{n-1} \end{bmatrix} = n$$

If a matrix P: $= Q + K^T RK$, where P is symmetric, substitute P and $u(\tau)$ in equation (2.2b) and simplify the function. Reference [20] provides the deviation and obtains the following matrix Riccati equation (2.3), there exists a limiting solution $P(t)$ to the Riccati equation.

$$-\dot{P} = A^T P + PA + Q - PBR^{-1}B^{-1}P \tag{2.3}$$

The matrix $P(t)$ is substituted into the optimal control law $u^*(t)$ and the state feedback gain (K) can be evaluated.

$$u^*(t) = R^{-1}(t)B^T P(t)x(t) = -K(t)x(t) \tag{2.4}$$

Figure 2.2 shows the gains calculated by the LQR ensure an optimal performance [21].

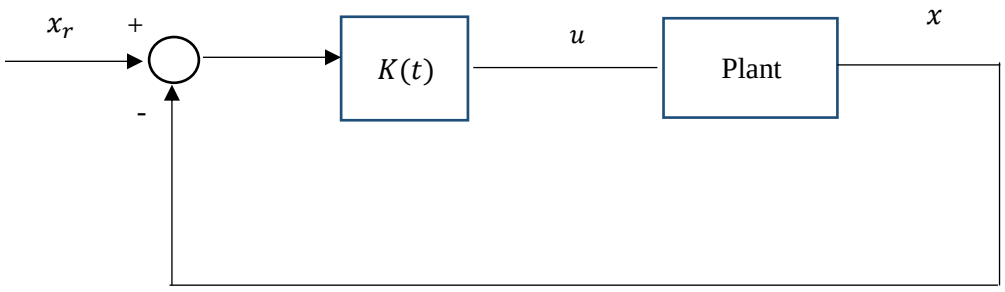

Figure 2.2 Optimal LQR State-Feedback Configuration

The initial value for the matrix Q and R can be chosen based on Bryson's rule [22] which chooses the diagonal values to be:

$$Q_{ii} = \frac{1}{\max x_i^2} \quad R_{jj} = \frac{1}{\max u_j^2} \tag{2.5}$$

Bryson's rule scales the variables so that the maximum accepted value for each term is 1. For higher order systems the LQR can then be tuned manually according to the results. If Q_{ii} is larger in comparison to R_{jj} than the state will be more penalized than the control.

Chapter 3
Design and Synchronization of a Microgrid

Note: Reproduced from Reference [23]

A MG can incorporate communication and controls to create a smarter, efficient, and robust grid. The purpose of this chapter is to design and integrate a MG into an existing campus expansion plan. Integrating a MG will improve reliability and resilience, as well as increase environmental and economic benefits. To validate the designed MG, a model of the MG is constructed in a Real Time Simulator Computer Aided Design (RSCAD) and is simulated using a Real Time Digital Simulator (RTDS). Two case studies are performed, including the synchronization and the battery assistance for frequency regulation. The simulation results show the feasibility of the designed MG.

3.1 Load Estimation

The MG under investigation will expand a storage yard into a campus to incorporate new buildings such as a district office, fleet maintenance garage, mobile unit storage, transmission overhead line maintenance facility, and a high voltage lab. To properly model the MG, the loads of these buildings need to be accurately estimated. To conduct load estimation watts / ft^2 was used to determine the total load. After taking into consideration the square footage of each building the total load was estimated to be 1.02MW.

Average Watts/Square Foot of Various Building Types (λ)	
Warehouse	0.82 watts / ft^2
Storage Unit	0.76 watts / ft^2
Maintenance Facility	6.7 watts / ft^2
Office Building	10 watts / ft^2

Table 3.1 Load Estimation Characteristics

$$Load(kw) = \lambda \times A \tag{3.1}$$

3.2 Photovoltaic Generation

Photovoltaic generation was chosen to be within this MG because it is environmentally friendly, and it is an inverter-based DG. A fixed tilt angle approach is applied in this case study. Equation (3.2a) was used to calculate the maximum solar power possible, where S_d is the daily solar constant, A_T is the atmospheric transmittance, L is the latitude of the location and θ_{Tilt}, δ are the tilt and declination angle [24]. The maximum power availability is determined when $(L - \theta_{Tilt}) = \delta$ .The declination angle varies seasonally $\pm 23.45°$ due to the tilt of the Earth on its axis of rotation and the rotation of the Earth around the sun. The maximum tilt angle is given in equation (3.2b) for the northern hemisphere. In [25] a formula is generated based on collected data for each combination of latitude and season. The date, latitude and the angle of the sun with respect to the panel determine the insolation. By observing the maximum insolation, the optimum tilt angles are calculated. A linear formula is determined based on the optimum dates and angles, as shown in equation (3.2c)

$$P = S_d A_T \left[\cos(L - \theta_{Tilt} - \delta)\right] \tag{3.2a}$$

$$\theta_{Tilt} = L - \delta \tag{3.2b}$$

$$\theta_{Tilt} = 3.1 + (L \times 0.76\,) \tag{3.2c}$$

Solar generation can be implemented in different ways such as rooftop, car port, and ground mounted, each with its own design specifications. To have the optimal output power from the PV panels, having the correct distance between each module in a row can avoid potential shading issues and generates the optimum output power. To determine the correct spacing between each module in a row a sunchart is utilized. The sunchart in Figure 3.1 shows the azimuth and solar elevation angles at a specific time of date and season. The sun casts the longest shadow at 9am and 3pm and so these angles are evaluated.

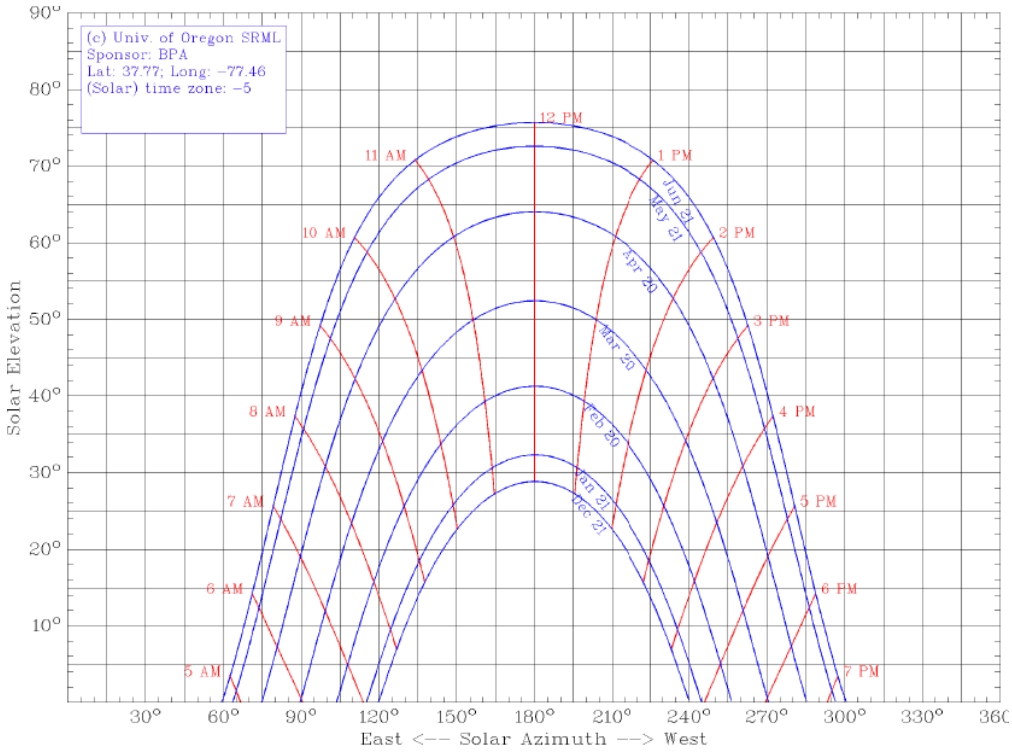

Figure 3.1 Sunchart for Campus [26]

Equations (3.3a-3.3c) were used to compute the space in between the row modules. The equations that determine the minimum row spacing X_{min} are represented by the following trigonometric equations.

$$H = sin(\theta_{Tilt}) \times W_{module} \tag{3.3a}$$

$$X = \frac{\Delta H}{tan(\theta_{se}\,)} \tag{3.3a}$$

$$X_{min} = Module\ Row\ Spacing \times cos(\theta_A) \tag{3.3c}$$

The following variables are defined: the width of the module W_{module}, solar elevation and azimuth angle θ_{se} and θ_A, module row spacing X, height H and the change of height ΔH. Based on the sunchart, the solar elevation angle and the azimuth angle are $\theta_{se} = 16°$ and $\theta_A = 135°$; the width module, W_{module}, utilized was 3.26ft. The computation of the minimum row spacing for the rooftop solar is found to be 4.45ft. The software program Helioscope is used to simplify the process of predicting the total output power based on the specifications. The total output power for rooftop solar is estimated to be 601.3kW [27]. The total generation capacity from ground mounted solar is found to be 394.2kW. The output power generated with the carports is projected to be 595kW. Overall, the total amount of PV generation predicted when including the solar carports, rooftop solar and grounded solar is 1.6MW.

3.3 Battery Energy Storage System

There are various reasons why utility companies are interested in a Battery Energy Storage System (BESS) in their electric grid. BESS are utilized for peak shaving, load levelling, frequency regulation, voltage regulation and peak shifting and load smoothing.

Peak Shaving: During peak hours the BESS operates in the discharging mode to reduce the power imported from the grid and lower peak demand. During the off-peak load period the BESS operates in the charging mode.

Load Levelling: Transient cloud movement can cause power fluctuations. BESS is designed to smooth out the PV array output and load by absorbing and delivering power such that the net power, which is the summation of the PV array, load power and battery, is relatively constant [28]. The BESS incorporated in this work is designed to assist frequency regulation when the MG is islanded.

Frequency Regulation: A variation of frequency in the power system is caused by the power mismatch between generation and the load demand. Since the inertia of the MG is small when the MG is islanded, it is very challenging to regulate the frequency of the MG. Due to the relatively fast response rate; BESS can help regulate frequency by absorbing real power when the MG frequency exceeds its threshold and inject real power when the MG frequency decreases below its threshold. In this model two lithium-ion phosphate batteries are used because of its safety record and robust life cycle [29]. Both batteries have an initial state of charge (SOC) of 85% and have a power rating of 0.58MWh [30]. The BESS size is chosen based on the maximum critical load. If the maximum critical load is uncertain, various methods can be used to find the optimal size of the BESS [31].

To regulate the frequency to 60 Hz an integral controller is implemented and designed to compensate for the frequency error. In Figure 2, the difference between ω_{ref} and ω_{gen} represents the angular frequency error. After converting the error to per unit it is multiplied by the integral controller gain based on equation 7 to calculate the additional active power needed to be provided by the battery to regulate the frequency at 60 Hz. This controller is implemented in the RTDS model.

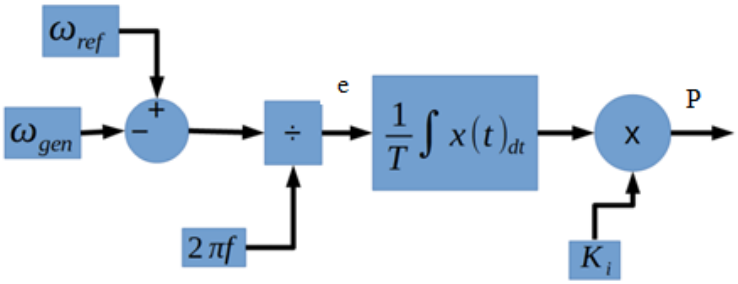

Figure 3.2 Frequency Controller

3.4 Real Time Digital Simulator Model

When selecting which bulk feeder will power the MG it is important to consider the topology of the substation. It is ideal to select two feeders, to add redundancy to the system. One of the cables used was the UG 1000 kcmil AL XLPE 35kV which has an impedance of $0.9821 + \mathrm{j}0.4794\ \Omega/m$. The other cable used is UG 1/0 3Ø AL XLPE 35kV and it has an impedance of $0.2101 + \mathrm{j}0.3047\ \Omega/m$. The line impedance can be calculated by knowing the length of the line and the impedance per mile of each cable type. The Real Time Simulator Computer Aided Design (RSCAD) model of the MG is shown in Figure 3.3. The circuit model was created in RSCAD based on the estimated load, predicted generation, the designed BESS and generator, and the line impedance calculations. The main grid has an impedance of $0.00347 + 0.04373j$ and the X/R ratio is 12.6. The RTDS operates in real time, allowing the user to interface physical equipment with the simulated model to test and validate the operation of MG protection and control devices under realistic conditions [32]. A 3-phase fault is simulated before the point of common coupling with a fault level of 250kA.

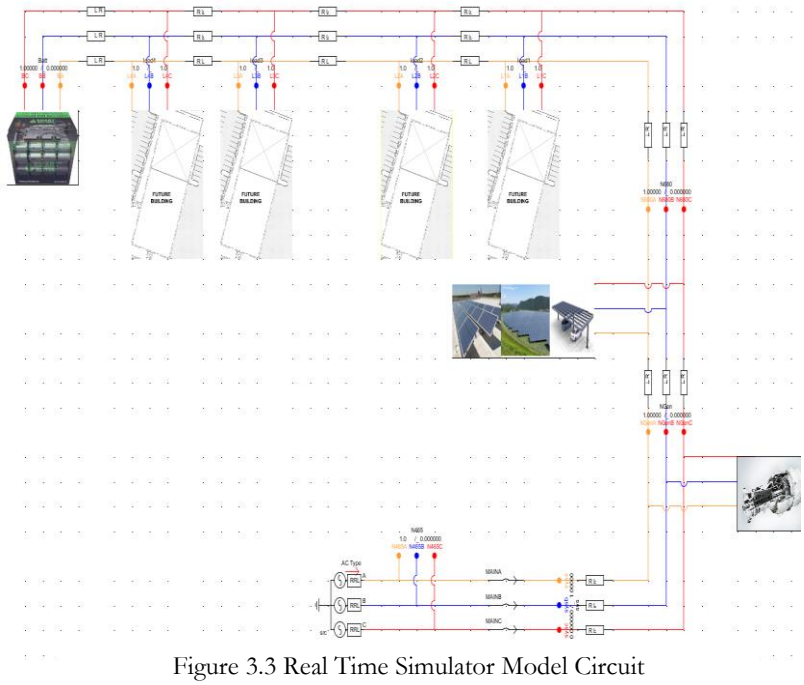

Figure 3.3 Real Time Simulator Model Circuit

3.4.1 Battery Storage used to support frequency regulation

As mentioned in section 3.3, the battery storage can help regulate the frequency due to its fast response time; the controls shown in Figure 3.2 are implemented in RSCAD, shown in Figure 3.4.

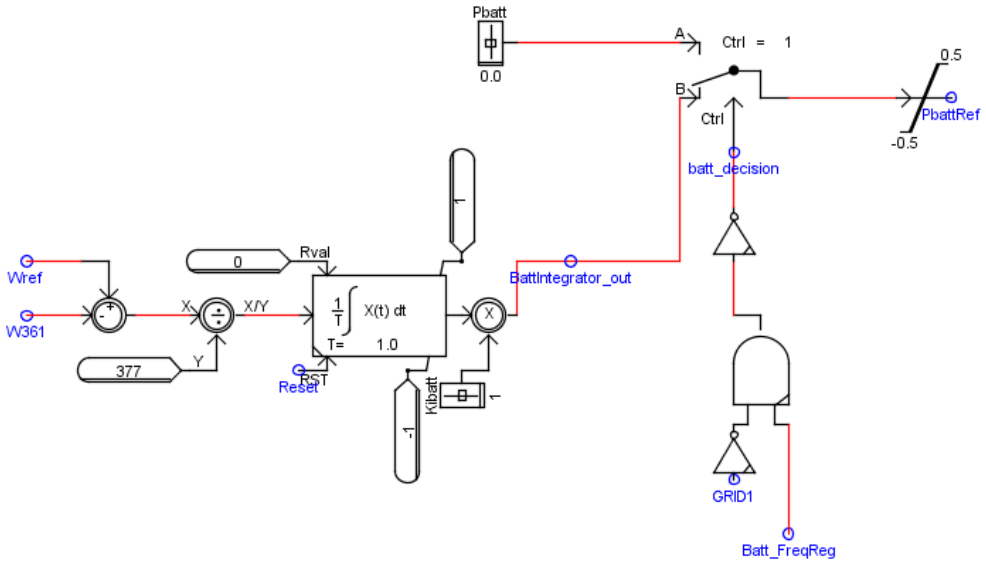

Figure 3.4 RTDS Frequency Control Circuit Model

In this case study the MG is in an islanded mode and the initial load is 0.68MW. During the simulation the load increases by 0.15MW. In the first scenario the battery storage is not used for the assistance of frequency regulation. Only the generator is used for frequency regulation. It takes the system 32 seconds to bring the frequency back to 60 Hz as shown in Figure 3.5.

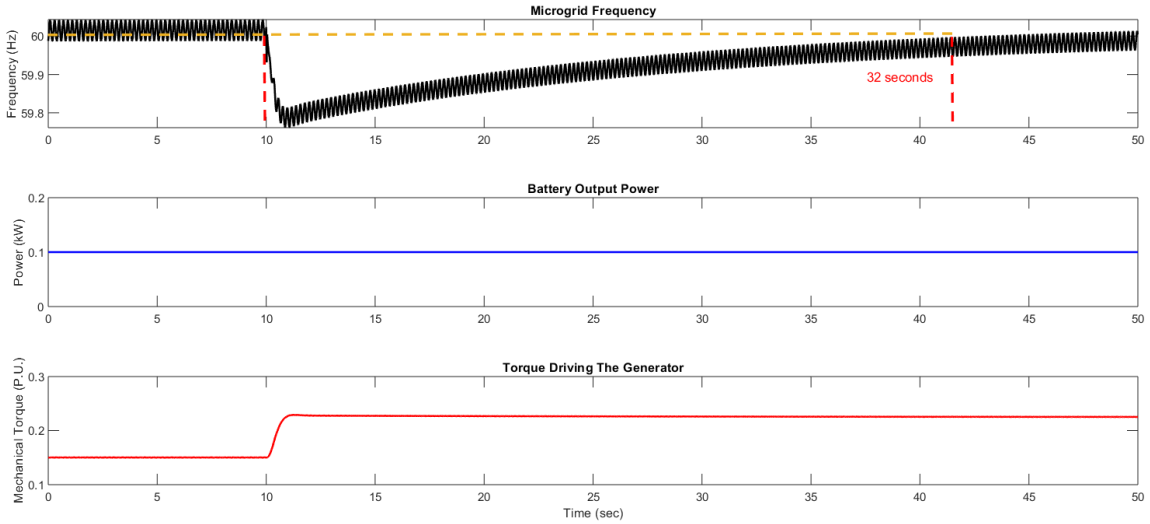

Figure 3.5 Generator used to regulate frequency

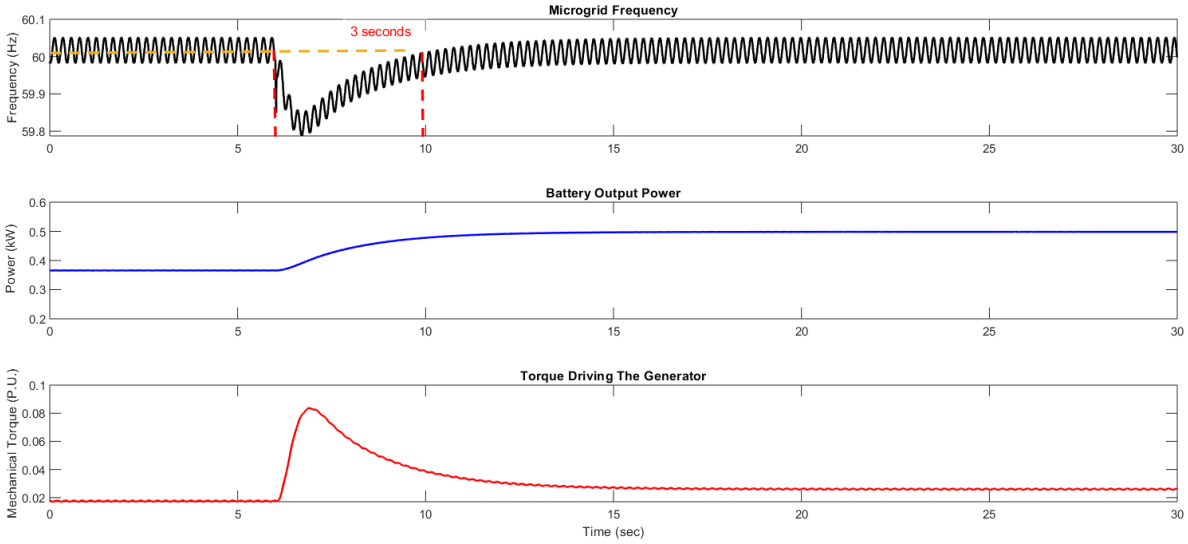

Figure 3.6 Generator and battery storage are used to regulate the frequency

In the second scenario, the battery storage is used to assist the generator to regulate the frequency. It can be observed that with the help of battery storage, the desired frequency regulation is achieved within 3 seconds, as shown in Figure 3.6.

3.4.2 Grid Synchronization

Synchronization of the MG to the electric grid is a crucial task. An abnormal synchronization can cause a disturbance in the system, damage equipment, and trigger relay operations. Since the systems rating of DER is between 500 and 1500 kVA it has a tolerance limit base on IEEE 1547 standard [5].

The tolerance limits for proper synchronization of a DER to an Electric Power System (EPS) are:

- Frequency difference: 0.2 Hz
- Voltage difference: 5%
- Phase angle difference: 15°

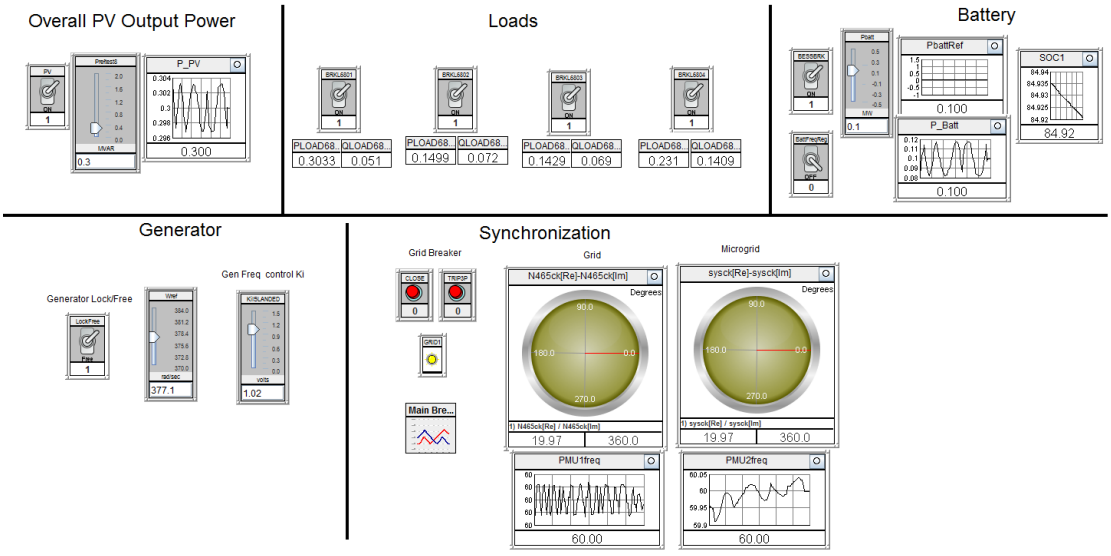

Figure 3.7 Run Time Controls

During the simulation the runtime file allows the user to control switches, sliders and buttons. The controls in Figure 3.7 are used to test the synchronization between the MG and electric grid. In this case study, a breaker command is given to synchronize the MG to the electric grid.

The synchro check relay (ANSI/IEEE device 25) is utilized in this case study. This relay can automate closing [33]. The relay will close the breaker when the input tolerance limits are satisfied and thus conducting synchronization. The parameters of the synchro-check element are shown in Figure 3.8.

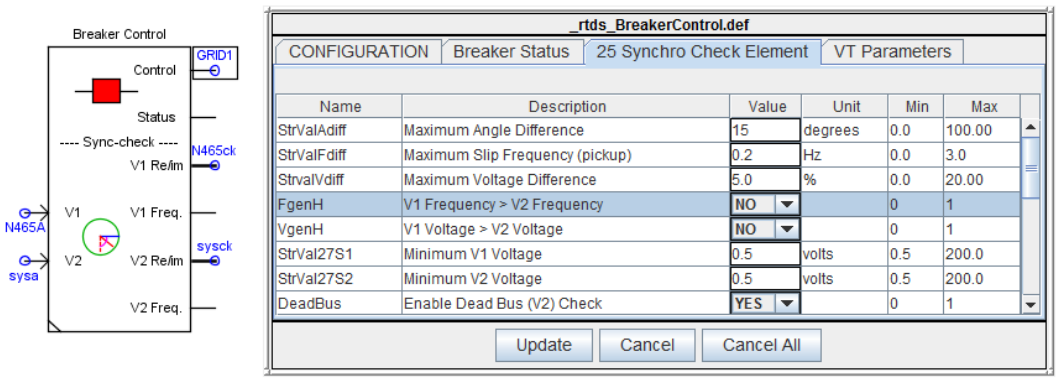

Figure 3.8 Relay Synchro check element

As can be seen in Figure 3.9, the breaker command is given at 1.97 seconds and the breaker closes at 2.49 seconds, when the tolerance criteria are met. Since there is a phase angle difference greater than 15° degrees the breaker does not close until the phase difference between the MG and the grid is 15° degrees or less.

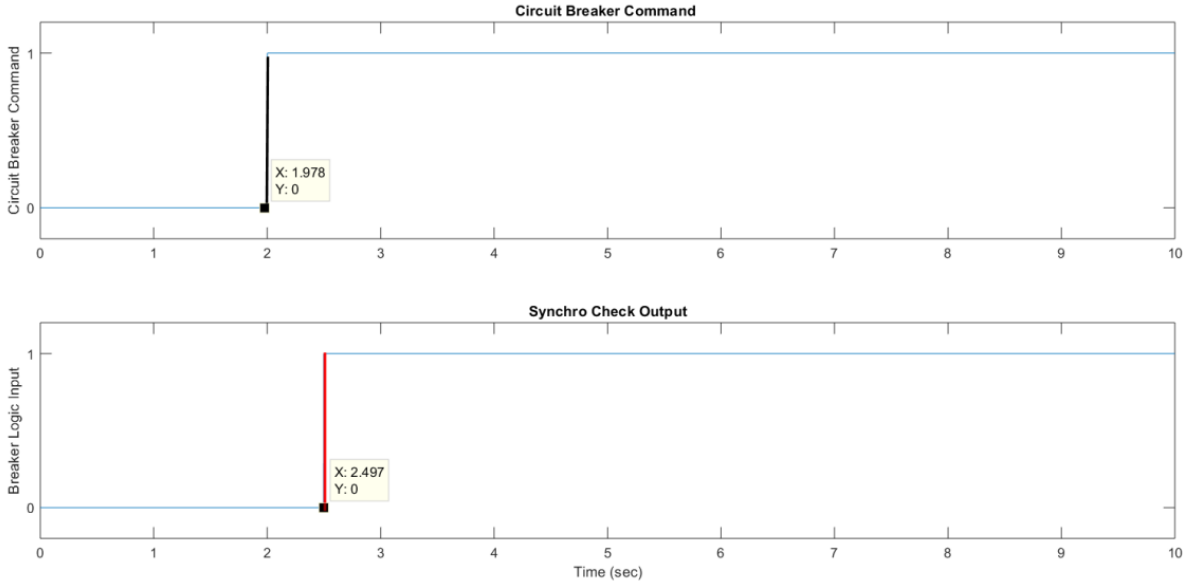

Figure 3.9 Circuit breaker Results

To correct the phase angle difference previously mentioned, the generators speed is increased, the blue line in Figure 3.10 shows this action. After this correction the phase, frequency and voltage difference are all within the required limits at 2.5 seconds and the MG and grid are synchronized.

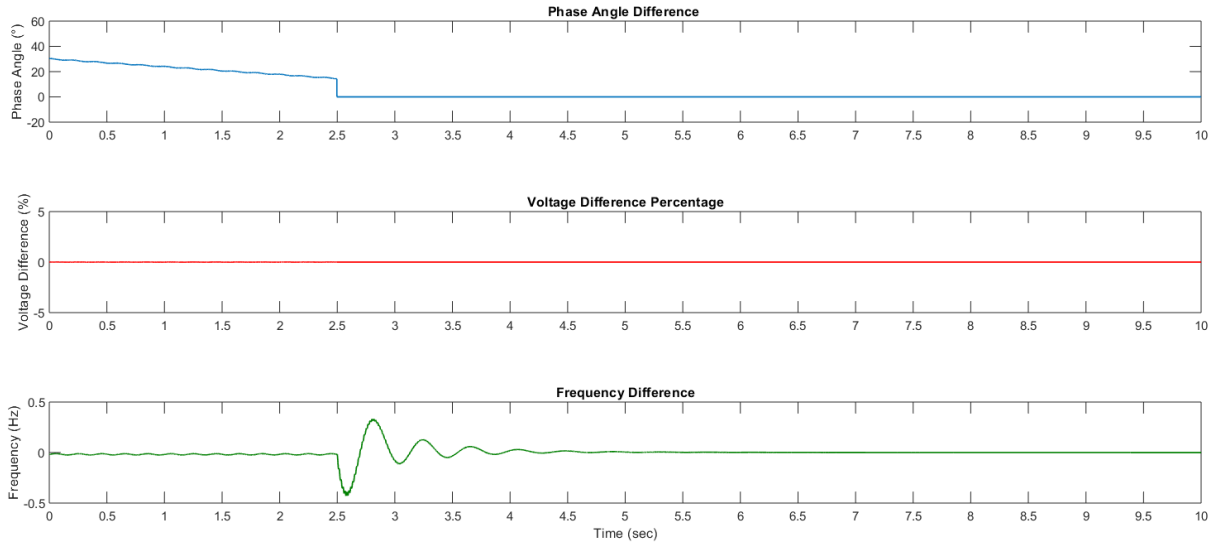

Figure 3.10 Synchronization Results

3.5 Conclusion

The need for a robust environmental and economically friendly system calls for the deployment of MGs. Due to the Grid Transformation & Security Act, Dominion Energy decided to launch a Microgrid Demonstration Project to gain real-world knowledge and experience associated with MGs [7]. The main goal of having MGs is to provide constant power for critical loads during outage events. The first step in the design process is to build a simulation model of the MG to analyze the challenges that lay ahead. This chapter focused on investigating the feasibility of implementing a MG at Dominion Energy owned facility/campus by conducting load estimation, designing PV generation and battery storage, and constructing a RTDS mode to run simulations on different case studies. Two case studies that were examined: synchronization of the MG to the grid and using battery storage to support frequency regulation. Based on the simulations above, it has been demonstrated that including a BESS will help the generator maintain the frequency within the permitted range and restore the frequency of the MG to the nominal value. Once the BSSE has a SOC of 20% then the battery will turn off, if the frequency still has a deviation from nominal frequency then the generator will continue to regulate the frequency. The future work includes conducting hardware-in-the-loop testing using relays required at the DG site as well as designing a comprehensive MG Controller that will coordinate and encompass the battery, PV and generator controller.

Chapter 4
Development of a Voltage and Current Controller for Critical Load Pick up

4.1 Introduction

As the distribution grid remains vulnerable to natural disasters and large faults it is important to focus on grid resilience. Quick mitigating strategies must be performed to enhance resiliency. MG can potentially be used as a resiliency source to serve critical loads. To restore as much load as possible frequency and voltage control must be conducted. Last chapter is focused on using a battery storage to help regulate frequency faster. This chapter is concerned with voltage and current control when restoring load. The proportional integral (PI) controller is used for the voltage control at PCC and the linear quadratic regulator (LQR) is implemented as the current control at the PCC within the MG. An average model in the D-Q frame is calculated to analyze the inherent dynamics of the current controller for the PCC. During normal operations this controller can also be utilized for other functions i.e. grid monitoring. To identify the grids topology in [34] the active and reactive power setpoints of the smart inverter are perturbed and the grid response (voltage) is recorded, which further calls for reliable controllers for the smart inverters in normal operation.

4.2 LCL Filter Design

The pulse width modulation (PWM) technique is used to control the output voltage or current. PWM varies the duty cycle at a high switching frequency which affects the duration of when the insulated-gate bipolar transistor (IGBT) is turned on or off. The duty cycle is based on the trains of switched pulses formed by comparing the triangular carrier waveform and the reference waveform. Since the IGBTs drive nonlinear loads, harmonics, integer multiplies of the fundamental frequency are produced. Having harmonics in the system causes distortion in the waveform, degrading the power quality. Increasing the switching frequency, however, can decrease the harmonic distortion and the harmonic components can be filtered with either a LC or LCL filter which is a low-pass filter. Many papers have reported different filter-designing process, e.g., [35-37]. In this research particularly, the procedure in reference [36] designs the LCL filter in a way that mitigates the harmonics from the inverter. Reference [36] is used to design the LCL filter in this research. The system parameters needed to design the LCL filter are included in Table 4.1. A current ripple of 10% is included in the LCL filter design. It is known that the maximum ripple current is produced when the modulation index equals 0.5; therefore, it is used within the design procedure. The capacitor C_f is designed so that the maximum power factor variation seen by the microgrid or grid is 5%. The resonance frequency and damping resistor of the filter are given by

$$\omega_{res} = \frac{\sqrt{L_1 + L_2}}{L_1 L_2 C_f} \tag{4.2a}$$

$$R_f = \frac{1}{3\omega_{res} C_f} \tag{4.2b}$$

The resonance frequency should be within this range

$$10\omega_n < \omega < 0.5\omega_{sw}$$

Symbol	Values	Description
V_{dc}	960V	DC Link Voltage
V_{LL}	480V	Line-To-line RMS Voltage
V_{ph}	277V	Phase Voltage
P_n	518kW	Rated Active Power
f_{sw}	10kHz	Switching Frequency
f_g	60Hz	Grid Frequency
f_{res}	4k	Resonance Frequency

Table 4.1 System Parameters

L_1 is the inductor connected to the inverter, L_2 is the inductor connected to the grid. C_f denotes the filter capacitor, R_f is the damping resistor, and R_1 and R_2 represent the internal resistors of the inductor. An LCL filter is connected in between the inverter and the rest of the microgrid. The values of the LCL filter are indicated in Table 4.2. The currents i_1, i_2 and i_f are the output current of the inverter, the microgrid current, and the capacitor current.

Symbol	Values
L_1	**0.18 mH**
L_2	**0.212 µH**
C_f	**0.298 mF**
R_f	**55.6 mΩ**

Table 4.2 Filter Parameters

For the nominal output power, the resistive load can be calculated:

$$R_{load} = \frac{V_0^2}{P} = \frac{480^2}{518\text{k}} = \ 0.44\Omega$$

4.3 Inverter Design While Connected to Generator

The power stage of the inverter consists of the BESS, inverter, LCL filter, maximum load and the voltage generation formed by the diesel generator as shown in Figure 4.1. The BSSE is represented by a voltage source, series resistor and the capacitor connected in parallel.

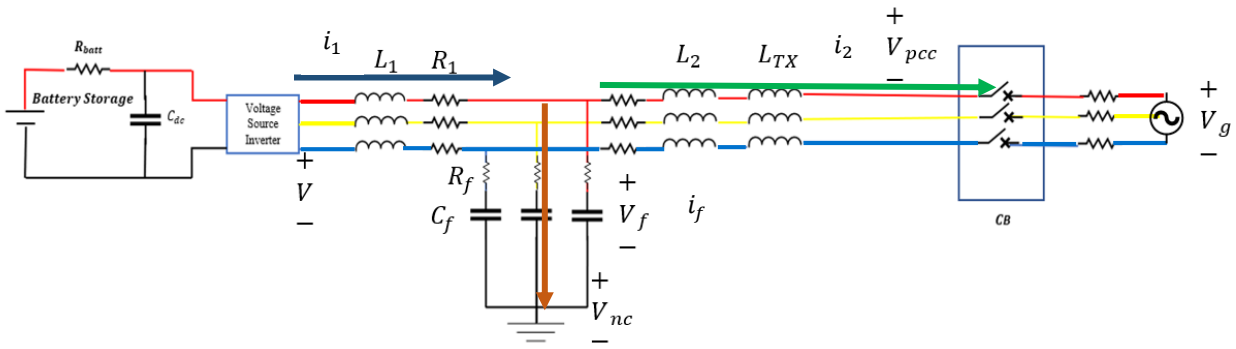

Figure 4.1 Three phase diagram of the power stage

An LCL filter is used to reduce the harmonics of the output current from the voltage source inverter that is connected to the energy storage system. L_1 and R_1 form the impedance connected to the inverter side.C_f and R_f are the shunt branch, L_2 and R_2 is the grid side impedance, L_{tx} is the transformer inductance, R_{Load} represents the maximum load the battery storage can provide for, V_{pcc} is the point of common coupling voltage, V_n is the neutral point and V_g is the voltage provided by the generator and, when it is connected to the grid V_g, is the grid voltage. i_1, i_2 and i_f are the inverter connected, grid connected, and shunt branch currents. The currents are depicted in Figure 4.1 and indicated by the blue, green and orange arrow, respectively.

4.3.1 Dynamic Equation

By using circuit analysis and Kirchhoff's law [38] left the following differential equations can be concluded:

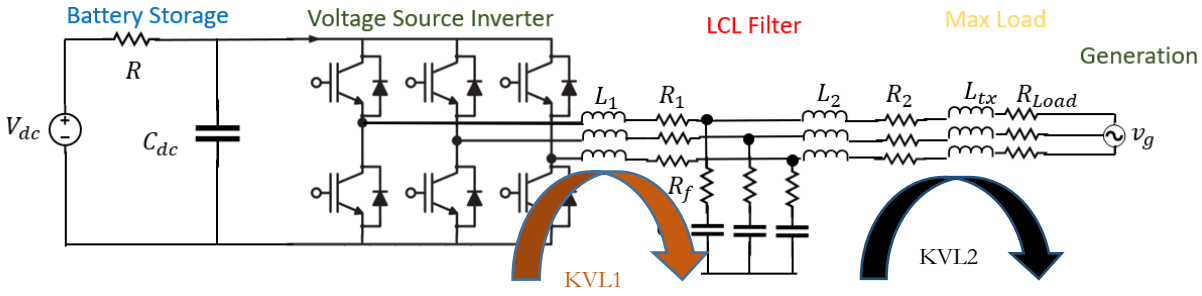

Figure 4.2 Battery Storage Inverter with LCL Filter Grid Connected

The switch input multiplied by the current or voltage is equivalent to the phase variable and vice versa as per equation (4.3a-4.3b). The switching model-phase variable is defined as [39]:

$$\begin{cases} i_{dc} = \vec{S}_{abc}^{T}\vec{i}_{2abc} \\ \vec{v}_{abc} = \vec{S}_{abc}v_{dc} \end{cases} \tag{4.3a}$$

The vectors in equation 4.3a are defined as:

$$\vec{v}_{abc} = \begin{bmatrix} v_{an} \\ v_{bn} \\ v_{cn} \end{bmatrix} \qquad \vec{s}_{abc} = \begin{bmatrix} s_a \\ s_b \\ s_c \end{bmatrix} \qquad \vec{i}_{abc} = \begin{bmatrix} i_{an} \\ i_{bn} \\ i_{cn} \end{bmatrix}$$

According to Kirchhoff voltage law the second loop that corresponds to the black arrow for phase a is:

$$-v_n - v_{f,a} + (L_2 + L_{tx} + L_{load})\frac{di_{2,a}}{dt} + (R_2 + R_{load})i_{2,a} + v_g = 0 \tag{4.31a}$$

After adding all three phases, the resulting equation is:

$$\begin{aligned} -3v_n - v_{f,a} - v_{f,b} - v_{f,c} + (L_2 + L_{tx} + L_{load}) \quad & \frac{d(i_{2,a} + i_{2,b} + i_{2,c})}{dt} \\ + (R_2 + R_{load})(i_{2,a} + i_{2,b} + i_{2,c}) + v_{g,a} + v_{g,b} + v_{g,c} &= 0 \end{aligned} \tag{4.31b}$$

The neutral point currents add to 0 since the three-phase system is balanced:

$$i_a + i_b + i_c = 0 \rightarrow \frac{di_a}{dt} + \frac{di_b}{dt} + \frac{di_c}{dt} = 0 \tag{4.31c}$$

After simplification and substituting (4.2c) into (4.2b) the following equation is:

$$-3v_n - v_{f,a} - v_{f,b} - v_{f,c} + v_{g,a} + v_{g,b} + v_{g,c} = 0$$

Solving for the neutral point v_n :

$$v_n = \frac{1}{3}(v_{g,a} + v_{g,b} + v_{g,c} - v_{f,a} - v_{f,b} - v_{f,c}) \tag{4.31d}$$

The voltage at the generator and the shunt branch voltage vectors are:

$$\vec{v}_g = \begin{bmatrix} v_{g,a} \\ v_{g,b} \\ v_{g,c} \end{bmatrix} \vec{v}_c = \begin{bmatrix} v_{c,a} \\ v_{c,b} \\ v_{c,c} \end{bmatrix}$$

4.3.1.A Inverter Side Current

Apply Kirchhoff voltage law for circuit analysis to the first loop that corresponds to the orange arrow in figure 4.2 for phase a is:

$$-v_a + L_1 \frac{di_{1,a}}{dt} + R_1 i_{1,a} + R_f(i_{1,a} - i_{2,a}) + v_{f,a} + v_n = 0 \tag{4.32a}$$

Substituting equation (4.2d) for v_n in equation (4.3a):

$$-v_a + L_1 \frac{di_{1,a}}{dt} + R_1 i_{1,a} + R_f(i_{1,a} - i_{2,a}) + v_{f,a} + \frac{1}{3}(v_g - v_f) = 0 \tag{4.32b}$$

The terms are reduced to the following equation:

$$-v_a + L_1 \frac{di_{1,a}}{dt} + R_1 i_{1,a} + R_f(i_{1,a} - i_{2,a}) + v_{f,a} + \frac{1}{3}(v_{th,a} + v_{th,b} + v_{th,c} - 2v_{f,a} - v_{f,b} - v_{f,c}) = 0$$

The purpose of doing the circuit analysis is to obtain the state-space representation of the model. Since the dynamic system is time-invariant the differential and algebraic equation is written in matrix form. The first order differential equation in the abc-frame for the current flowing from the inverter is:

$$\frac{di_{1,a}}{dt} = \frac{1}{L_1}(v_a - (R_1 + R_f)i_{1,a} + R_f i_{2,a} - \frac{1}{3L_1}(v_{g,a} + v_{g,b} + v_{g,c}) - \frac{1}{3L_1}(2v_{f,a} - v_{f,b} - v_{f,c}) \tag{4.3c}$$

The same process for the a-phase is applied for the b-phase and c-phase. Theses equations are then put into matrix form

$$\frac{d}{dt}\begin{bmatrix} i_{1a} \\ i_{1b} \\ i_{1c} \end{bmatrix} = \frac{1}{L_1}\begin{bmatrix} v_a \\ v_b \\ v_c \end{bmatrix} + \begin{bmatrix} -\frac{R_1+R_f}{L_1} & 0 & 0 \\ 0 & -\frac{R_1+R_f}{L_1} & 0 \\ 0 & 0 & -\frac{R_1+R_f}{L_1} \end{bmatrix}\begin{bmatrix} i_{1a} \\ i_{1b} \\ i_{1c} \end{bmatrix} + \frac{R_f}{L_2}\begin{bmatrix} i_{2a} \\ i_{2b} \\ i_{2c} \end{bmatrix} + \frac{1}{3L_1}\begin{bmatrix} 1 & 1 & 1 \\ 1 & 1 & 1 \\ 1 & 1 & 1 \end{bmatrix}\begin{bmatrix} v_{g,a} \\ v_{g,b} \\ v_{g,c} \end{bmatrix} + \frac{1}{3L_1}\begin{bmatrix} -2 & 1 & 1 \\ 1 & -2 & 1 \\ 1 & 1 & -2 \end{bmatrix}\begin{bmatrix} v_{fa} \\ v_{fb} \\ v_{fc} \end{bmatrix} \tag{4.33}$$

As mentioned in chapter 2 to simplify the analysis of three- phase system and the calculations for the controller, transforming the system to the $dq0$ frame is ideal.

Consider the Clark and Park transformation:

$$T_n = T_{dq0\backslash abc} = \sqrt{\frac{2}{3}}\begin{bmatrix} cos(\omega t) & cos(\omega t - \frac{2\pi}{3}) & cos(\omega t + \frac{2}{3}\pi) \\ -sin(\omega t) & -sin(\omega t - \frac{2\pi}{3}) & -sin(\omega t + \frac{2\pi}{3}) \\ \frac{1}{\sqrt{2}} & \frac{1}{\sqrt{2}} & \frac{1}{\sqrt{2}} \end{bmatrix} \quad \& \quad T_n^{-1} = T_{dq0\backslash abc}^{-1}$$

$$\bar{\imath}_{1dq0} = \begin{bmatrix} \bar{\imath}_{1d} \\ \bar{\imath}_{1q} \\ \bar{\imath}_{10} \end{bmatrix} \quad \bar{v}_{g,dq0} = \begin{bmatrix} \bar{v}_{g,d} \\ \bar{v}_{g,q} \\ \bar{v}_{g,0} \end{bmatrix}$$

Replace x_{abc} with $T_n^{-1}x_{dq0}$

$$\frac{d\left(T_n^{-1}\bar{\imath}_{L1dq0}\right)}{dt} = -\frac{(R_1+R_f)}{L_1}T_n^{-1}\bar{\imath}_{1dq0} + R_f T_n^{-1}\bar{\imath}_{2dq0} + \frac{1}{3L_1}\begin{bmatrix} 1 & 1 & 1 \\ 1 & 1 & 1 \\ 1 & 1 & 1 \end{bmatrix} T_n^{-1}\,\bar{v}_{th,dq0} + \frac{1}{3L_1}\begin{bmatrix} -2 & 1 & 1 \\ 1 & -2 & 1 \\ 1 & 1 & -2 \end{bmatrix} T_n^{-1}\bar{v}_c$$

$$\frac{d}{dt}[\,T_n^{-1}]\begin{bmatrix} \bar{\imath}_{L1d} \\ \bar{\imath}_{L1q} \\ \bar{\imath}_{L10} \end{bmatrix} + [\,T_n^{-1}]\,\frac{d}{dt}\begin{bmatrix} \bar{\imath}_{1d} \\ \bar{\imath}_{1q} \\ \bar{\imath}_{10} \end{bmatrix} = -\frac{(R_1+R_f)}{L_1}T_n^{-1}\bar{\imath}_{1dq0} + R_f T_n^{-1}\bar{\imath}_{2dq0} + \frac{1z}{3L_1}\begin{bmatrix} 1 & 1 & 1 \\ 1 & 1 & 1 \\ 1 & 1 & 1 \end{bmatrix} T_n^{-1}\bar{v}_{g,dq0} + \frac{1}{3L_1}\begin{bmatrix} -2 & 1 & 1 \\ 1 & -2 & 1 \\ 1 & 1 & -2 \end{bmatrix} T_n^{-1}\bar{v}_{fdq0}$$

Multiply both sides by T_n to simplify:

$$T_n \frac{d}{dt}[T_n^{-1}]\begin{bmatrix}\bar{\imath}_{L1d}\\ \bar{\imath}_{L1q}\\ \bar{\imath}_{L10}\end{bmatrix} + \frac{d}{dt}\begin{bmatrix}\bar{\imath}_{L1d}\\ \bar{\imath}_{L1q}\\ \bar{\imath}_{L10}\end{bmatrix}$$
$$= -\frac{(R_1+R_f)}{L_1}\bar{\imath}_{1dq0} + R_f\bar{\imath}_{2dq0} + \frac{1}{3L_1}T_n\begin{bmatrix}1 & 1 & 1\\ 1 & 1 & 1\\ 1 & 1 & 1\end{bmatrix}T_n^{-1}\vec{d}_{phdq0}\bar{v}_{dc}$$
$$+\frac{1}{3L_1}T_n\begin{bmatrix}-2 & 1 & 1\\ 1 & -2 & 1\\ 1 & 1 & -2\end{bmatrix}T_n^{-1}\bar{v}_{fdq0}$$

$$\frac{d}{dt}\begin{bmatrix}\bar{\imath}_{L1d}\\ \bar{\imath}_{L1q}\\ \bar{\imath}_{L10}\end{bmatrix} = -\frac{R_1+R_f}{L_1}\bar{\imath}_{1dq0} - T_n\frac{d}{dt}[T_n^{-1}]\begin{bmatrix}\bar{\imath}_{L1d}\\ \bar{\imath}_{L1q}\\ \bar{\imath}_{L10}\end{bmatrix} + R_f\bar{\imath}_{2dq0} + \frac{1}{3L_1}T_n\begin{bmatrix}1 & 1 & 1\\ 1 & 1 & 1\\ 1 & 1 & 1\end{bmatrix}T_n^{-1}\vec{d}_{phdq0}\bar{v}_{dc}$$
$$+\frac{1}{3L_1}T_n\begin{bmatrix}-2 & 1 & 1\\ 1 & -2 & 1\\ 1 & 1 & -2\end{bmatrix}T_n^{-1}\bar{v}_{fdq0}$$

Assuming this is a balance system one can assume $cos(\omega t) + cos\left(\omega t - \frac{2\pi}{3}\right) + cos\left(\omega t + \frac{2}{3}\pi\right)$

$$3I - \frac{2}{3}\begin{bmatrix}cos(\omega t) & cos\left(\omega t - \frac{2\pi}{3}\right) & cos\left(\omega t + \frac{2}{3}\pi\right)\\ -sin(\omega t) & -sin\left(\omega t - \frac{2\pi}{3}\right) & -sin\left(\omega t + \frac{2\pi}{3}\right)\\ \frac{1}{\sqrt{2}} & \frac{1}{\sqrt{2}} & \frac{1}{\sqrt{2}}\end{bmatrix}\begin{bmatrix}0 & 0 & \frac{3}{\sqrt{2}}\\ 0 & 0 & \frac{3}{\sqrt{2}}\\ 0 & 0 & \frac{3}{\sqrt{2}}\end{bmatrix} = \begin{bmatrix}3 & 0 & 0\\ 0 & 3 & 0\\ 0 & 0 & 0\end{bmatrix}$$

Repeat the same process for:

$$T_n\begin{bmatrix}-2 & 1 & 1\\ 1 & -2 & 1\\ 1 & 1 & -2\end{bmatrix}T_n^{-1} = \begin{bmatrix}-3 & 0 & 0\\ 0 & -3 & 0\\ 0 & 0 & 0\end{bmatrix}$$

It is known that:

$$T_n\frac{d}{dt}[T_n^{-1}] = \begin{bmatrix}0 & -\omega & 0\\ \omega & 0 & 0\\ 0 & 0 & 0\end{bmatrix}$$

$$T_n\begin{bmatrix}1 & 1 & 1\\ 1 & 1 & 1\\ 1 & 1 & 1\end{bmatrix}[T_n^{-1}] = \begin{bmatrix}0 & 0 & 0\\ 0 & 0 & 0\\ 0 & 0 & 3\end{bmatrix}$$

$$T_n\begin{bmatrix}-2 & 1 & 1\\ 1 & -2 & 1\\ 1 & 1 & -2\end{bmatrix}[T_n^{-1}] = \begin{bmatrix}-3 & 0 & 0\\ 0 & -3 & 0\\ 0 & 0 & 0\end{bmatrix}$$

The $dq0$ frame of the current flowing from the inverter yields to equation (4.5)

$$\frac{d}{dt}\begin{bmatrix}\bar{\imath}_{1d}\\ \bar{\imath}_{1q}\\ \bar{\imath}_{10}\end{bmatrix} = \frac{1}{L_1}\bar{v}_{dq0} + \begin{bmatrix}-\frac{R_1+R_f}{L_1} & \omega_g & 0\\ -\omega_g & -\frac{R_1+R_f}{L_1} & 0\\ 0 & 0 & -\frac{R_1+R_f}{L_1}\end{bmatrix}\bar{\imath}_{1,dq0} + \frac{R_f}{L_1}\bar{\imath}_{2dq0} - \frac{1}{L_1}\begin{bmatrix}1 & 0 & 0\\ 0 & 1 & 0\\ 0 & 0 & 0\end{bmatrix}\bar{v}_{f,dq0} \quad (4.5)$$

The d and q channel equations for the inverter sides inductors are:

$$\frac{di_{1,d}}{dt} = \frac{1}{L_1}(v_d - (R_1 + R_f)i_{1,d} + \omega L_1 i_{1,q} - v_{f,d}) \tag{4.6}$$

$$\frac{di_{1,q}}{dt} = \frac{1}{L_1}(v_q - (R_1 + R_f)i_{1,q} + \omega L_1 i_{1,d} - v_{f,q}) \tag{4.7}$$

4.3.1.B Generator Side Current

Circuit analysis is conducted for the generator side current in the case that the circuit breaker is closed, this corresponds to the black arrow for the KVL2 loop depicted in Figure 4.2

$$-v_n - v_{f,a} - R_f(i_1 - i_2) + R_2 i_2 + L_2\frac{di_2}{dt} + v_g = 0 \tag{4.8a}$$

The neutral voltage was previously defined in (4.2d) After substituting the new equation is

$$-\frac{1}{3}(v_{g,a} + v_{g,b} + v_{g,c} - v_{f,a} - v_{f,b} - v_{f,c}) - v_{f,a} - R_f(i_1 - i_2) + R_2 i_2 + L_2\frac{di_2}{dt} + v_{g,a} = 0$$

Solving for $\frac{di_2}{dt}$, it is obtained that

$$\frac{di_2}{dt} = \frac{1}{L_2}(\frac{1}{3}\left(v_{g,a} + v_{g,b} + v_{g,c} - v_{f,a} - v_{f,b} - v_{f,c}\right) + v_{f,a} + R_f(i_1 - i_2) - R_2 i_2 - v_{,a})$$

$$\frac{di_2}{dt} = \frac{1}{L_2}\left(\frac{2v_{f,a} - v_{f,b} - v_{f,c}}{3}\right) - (\frac{2v_{g,a} - v_{g,b} - v_{g,c}}{3}) + R_f(i_1 - i_2) - R_2 i_2) \tag{4.9}$$

Incorporate the inductance of the transformer in series and load by adding it the to existing L_2 and R_2.

$$L_{tot} = L_2 + L_{tx} + L_{load} \qquad R_{tot} = R_2 + R_{load}$$

The same process for the a-phase is applied for the b-phase and c-phase. Theses equations are then cast into a matrix form

$$\frac{d}{dt}\begin{bmatrix}\bar{\imath}_{2a}\\ \bar{\imath}_{2b}\\ \bar{\imath}_{2c}\end{bmatrix} = \begin{bmatrix}\frac{-(R_{tot}+R_f)}{L_{tot}} & 0 & 0\\ 0 & \frac{-(R_{tot}+R_f)}{L_{tot}} & 0\\ 0 & 0 & \frac{-(R_{tot}+R_f)}{L_{tot}}\end{bmatrix}\begin{bmatrix}\bar{\imath}_{2a}\\ \bar{\imath}_{2b}\\ \bar{\imath}_{2c}\end{bmatrix} + \frac{R_f}{L_{tot}} i_{1,abc} - \frac{1}{3L_{tot}}\begin{bmatrix}2 & -1 & -1\\ -1 & 2 & -1\\ -1 & -1 & 2\end{bmatrix}\bar{v}_g - \frac{1}{3L_{tot}}\begin{bmatrix}-2 & 1 & 1\\ 1 & -2 & 1\\ 1 & 1 & -2\end{bmatrix}\overline{v_f} \tag{4.10a}$$

By applying the dq transformation:

$$\frac{d}{dt}\begin{bmatrix}\bar{\imath}_{2d}\\ \bar{\imath}_{2q}\\ \bar{\imath}_{20}\end{bmatrix}=\begin{bmatrix}\frac{-(R_{tot}+R_f)}{L_{tot}} & \omega_g & 0\\ -\omega_g & \frac{-(R_{tot}+R_f)}{L_{tot}} & 0\\ 0 & 0 & \frac{-(R_{tot}+R_f)}{L_{tot}}\end{bmatrix}\begin{bmatrix}\bar{\imath}_{2d}\\ \bar{\imath}_{2q}\\ \bar{\imath}_{20}\end{bmatrix}+\frac{R_f}{L_{tot}}i_{1,dq0}$$
$$-\frac{1}{L_{tot}}\begin{bmatrix}1&0&0\\0&1&0\\0&0&0\end{bmatrix}\bar{v}_{g,dq0}+\frac{1}{L_{tot}}\begin{bmatrix}1&0&0\\0&1&0\\0&0&0\end{bmatrix}\bar{v}_{f,dq0} \tag{4.10b}$$

The d and q channel equations for the grid side inductors is:

$$\frac{di_{2,d}}{dt}=\frac{1}{L_{tot}}(v_f+R_f i_{1,d}-(R_{tot}+R_f)i_{2,d}+\omega L_{tot}i_{2,q}-v_{g,d}) \tag{4.10c}$$

$$\frac{di_{2,q}}{dt}=\frac{1}{L_{tot}}(v_f+R_f i_{1,q}-(R_{tot}+R_f)i_{2,q}-\omega L_{tot}i_{2,d}-v_{g,q}) \tag{4.10d}$$

4.3.1.C Shunt Branch Voltage

KCL is also applied to the shunt brank voltage as indicated by the dark blue arrows in Figure 4.2

$$i_{2,a}=i_{1,a}+i_{f,a} \tag{4.11a}$$

$i_{f,a}$ can also be defined as

$$i_{f,a}=\frac{C_f dv_{f,a}}{dt} \tag{4.11b}$$

Substituting (4.11b) into (4.11a) results to

$$i_{2,a}=i_{1,a}+\frac{C_f dv_{f,a}}{dt} \tag{4.11c}$$

The voltage across the capacitor is defined as v_f. Then,

$$\frac{dv_f}{dt}=\frac{1}{C_f}i_{1_{abc}}-\frac{1}{C_f}i_{2_{abc}} \tag{4.11d}$$

$$\overline{v_c} = \begin{bmatrix} \bar{v}_{ca} \\ \bar{v}_{cb} \\ \bar{v}_{cc} \end{bmatrix} \qquad \bar{v}_g = \begin{bmatrix} v_{ga} \\ v_{gb} \\ v_{gc} \end{bmatrix} \qquad \vec{d}_{ph} = \begin{bmatrix} d_a \\ d_b \\ d_c \end{bmatrix}$$

$$\frac{d}{dt}\left[T_n^{-1}\bar{v}_{cdq0}\right] = \frac{1}{C_f}T_n^{-1}\begin{bmatrix} \bar{\imath}_{1d} \\ \bar{\imath}_{1q} \\ \bar{\imath}_{10} \end{bmatrix} - \frac{1}{C_f}T_n^{-1}\begin{bmatrix} \bar{\imath}_{2d} \\ \bar{\imath}_{2q} \\ \bar{\imath}_{20} \end{bmatrix}$$

Since T_n^{-1} is not a matrix of constants, chain rule theorem is applied:

$$\frac{d}{dt}[T_n^{-1}]\begin{bmatrix} \bar{v}_{f,d} \\ \bar{v}_{f,q} \\ \bar{v}_{f,0} \end{bmatrix} + T_n^{-1}\frac{d}{dt}\begin{bmatrix} \bar{v}_{f,d} \\ \bar{v}_{f,q} \\ \bar{v}_{f,0} \end{bmatrix} = \frac{1}{C_f}T_n^{-1}\begin{bmatrix} \bar{\imath}_{1d} \\ \bar{\imath}_{1q} \\ \bar{\imath}_{10} \end{bmatrix} - \frac{1}{C_f}T_n^{-1}\begin{bmatrix} \bar{\imath}_{2d} \\ \bar{\imath}_{2q} \\ \bar{\imath}_{20} \end{bmatrix}$$

Multiply both sides by T_n:

$$T_n\frac{d}{dt}[T_n^{-1}]\begin{bmatrix} \bar{v}_{f,d} \\ \bar{v}_{f,q} \\ \bar{v}_{f,o} \end{bmatrix} + \frac{d}{dt}\begin{bmatrix} \bar{v}_{f,d} \\ \bar{v}_{f,q} \\ \bar{v}_{f,o} \end{bmatrix} = \frac{1}{C_f}T_n\frac{d}{dt}[T_n^{-1}]\begin{bmatrix} \bar{\imath}_{1d} \\ \bar{\imath}_{1q} \\ \bar{\imath}_{1o} \end{bmatrix} - \frac{1}{C_f}T_n\frac{d}{dt}[T_n^{-1}]\begin{bmatrix} \bar{\imath}_{2d} \\ \bar{\imath}_{2q} \\ \bar{\imath}_{2o} \end{bmatrix}$$

Since:

$$T_n\frac{d}{dt}[T_n^{-1}] = \begin{bmatrix} 0 & -\omega & 0 \\ \omega & 0 & 0 \\ 0 & 0 & 0 \end{bmatrix}$$

Therefore:

$$\frac{d}{dt}\begin{bmatrix} \bar{v}_{fd} \\ \bar{v}_{fq} \\ \bar{v}_{f0} \end{bmatrix} = \frac{1}{C}\begin{bmatrix} \bar{\imath}_{1d} \\ \bar{\imath}_{1q} \\ \bar{\imath}_{10} \end{bmatrix} - \frac{1}{C}\begin{bmatrix} \bar{\imath}_{2d} \\ \bar{\imath}_{2q} \\ \bar{\imath}_{20} \end{bmatrix} - \begin{bmatrix} 0 & -\omega & 0 \\ \omega & 0 & 0 \\ 0 & 0 & 0 \end{bmatrix}\begin{bmatrix} \bar{v}_{fd} \\ \bar{v}_{fq} \\ \bar{v}_{f0} \end{bmatrix} \tag{4.12a}$$

The d and q channel equations for the shunt branch is:

$$\frac{dv_{f,d}}{dt} = \frac{1}{C_f}(i_{1d} - i_{2,d} + \omega C_f v_{f,q}) \tag{4.12b}$$

$$\frac{dv_{f,q}}{dt} = \frac{1}{C_f}(i_{1,q} - i_{2,q} - \omega C_f v_{f,d}) \tag{4.12c}$$

The following is the result of the state space representation when the circuit breaker is closed.

-

$$A = \begin{bmatrix} \frac{-(R_1+R_f)}{L_1} & \omega_g & \frac{R_f}{L_1} & 0 & \frac{-1}{L_1} & 0 & 0 \\ -\omega_g & \frac{-(R_1+R_f)}{L_1} & 0 & \frac{R_f}{L_1} & 0 & -\frac{1}{L_1} & 0 \\ \frac{R_f}{L_{tot}} & 0 & \frac{-(R_{tot}+R_f)}{L_{tot}} & \omega_g & \frac{1}{L_{tot}} & 0 & 0 \\ 0 & \frac{R_f}{L_{tot}} & -\omega_g & \frac{-(R_{tot}+R_f)}{L_{tot}} & 0 & \frac{1}{L_{tot}} & 0 \\ \frac{1}{C_f} & 0 & -\frac{1}{C_f} & 0 & 0 & \omega_g & 0 \\ 0 & \frac{1}{C_f} & 0 & -\frac{1}{C_f} & -\omega_g & 0 & 0 \end{bmatrix} \quad \vec{x} = \begin{bmatrix} \bar{i}_{1,d} \\ \bar{i}_{1,q} \\ \bar{i}_{2,d} \\ \bar{i}_{2,q} \\ \bar{v}_{f,d} \\ \bar{v}_{f,q} \end{bmatrix}$$

$$B = \begin{bmatrix} 0 & 0 & \frac{V_{dc}}{L_1} & 0 \\ 0 & 0 & 0 & \frac{V_{dc}}{L_1} \\ -\frac{1}{L_{tot}} & 0 & 0 & 0 \\ 0 & -\frac{1}{L_{tot}} & 0 & 0 \\ 0 & 0 & -\frac{i_{1,d}}{C_{dc}} & -\frac{i_{1,q}}{C_{dc}} \\ 0 & 0 & 0 & 0 \end{bmatrix} \quad \vec{u} = \begin{bmatrix} \tilde{v}_{g,d} \\ \tilde{v}_{g,q} \\ \tilde{d}_d \\ \tilde{d}_q \end{bmatrix}$$

(4.2)

4.3.2 Inverter Design Disconnected from the Generator

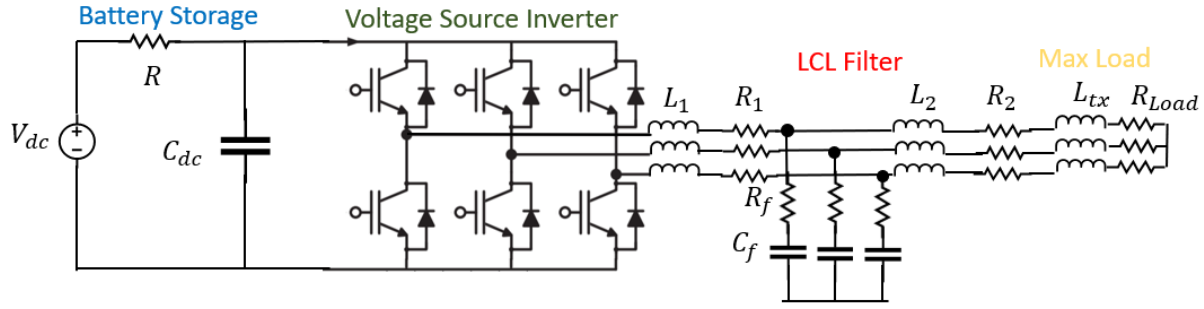

Figure 4.3 Battery Storage Inverter with LCL Filter

In the situation where the diesel generator or utility grid is unavailable, applying a similar circuit analysis as 4.3.1 will result in the following state space representation while the circuit breaker is open.

$$A = \begin{bmatrix} \frac{-(R_1+R_f)}{L_1} & \omega_g & \frac{R_f}{L_1} & 0 & \frac{-1}{L_1} & 0 & 0 \\ -\omega_g & \frac{-(R_1+R_f)}{L_1} & 0 & \frac{R_f}{L_1} & 0 & -\frac{1}{L_1} & 0 \\ \frac{R_f}{L_{tot}} & 0 & \frac{-(R_{tot}+R_f)}{L_{tot}} & \omega_g & \frac{1}{L_{tot}} & 0 & 0 \\ 0 & \frac{R_f}{L_{tot}} & -\omega_g & \frac{-(R_{tot}+R_f)}{L_{tot}} & 0 & \frac{1}{L_{tot}} & 0 \\ \frac{1}{C_f} & 0 & -\frac{1}{C_f} & 0 & 0 & \omega_g & 0 \\ 0 & \frac{1}{C_f} & 0 & -\frac{1}{C_f} & -\omega_g & 0 & 0 \end{bmatrix} \quad \vec{x} = \begin{bmatrix} \bar{\imath}_{1,d} \\ \bar{\imath}_{1,q} \\ \bar{\imath}_{2,d} \\ \bar{\imath}_{2,q} \\ \bar{v}_{f,d} \\ \bar{v}_{f,q} \end{bmatrix} \tag{4.3}$$

$$B = \begin{bmatrix} \frac{V_{dc}}{L_1} & 0 \\ 0 & \frac{V_{dc}}{L_1} \\ 0 & 0 \\ 0 & 0 \\ 0 & 0 \\ 0 & 0 \end{bmatrix} \quad \vec{u} = \begin{bmatrix} \bar{d}_d \\ \bar{d}_q \end{bmatrix} \qquad D = \begin{bmatrix} 0 & 0 \\ 0 & 0 \\ 0 & 0 \\ 0 & 0 \\ 0 & 0 \end{bmatrix}$$

4.4 Design approach for current controller

To enhance the systems stability an LQR controller is used for the current controller. When designing the current controller, it is assumed that all state variables are accessible as feedback measurements. In the case that the state variables are unavailable then they need to be estimated using a state observer which estimates the state variables based on the output and control measurements. This system is a linear time-invariant system and while connected to the diesel generator it can be expressed as

$$\dot{x} = Ax + Bu + Dv \tag{4.4a}$$

$$y = Cx \tag{4.4b}$$

$$u = -k_s x + k_I \varepsilon \tag{4.4c}$$

$$\dot{\varepsilon} = r - y = r - Cx \tag{4.4d}$$

The equations (4.4a-4.4d) are obtained for the system in Figure 4.4a

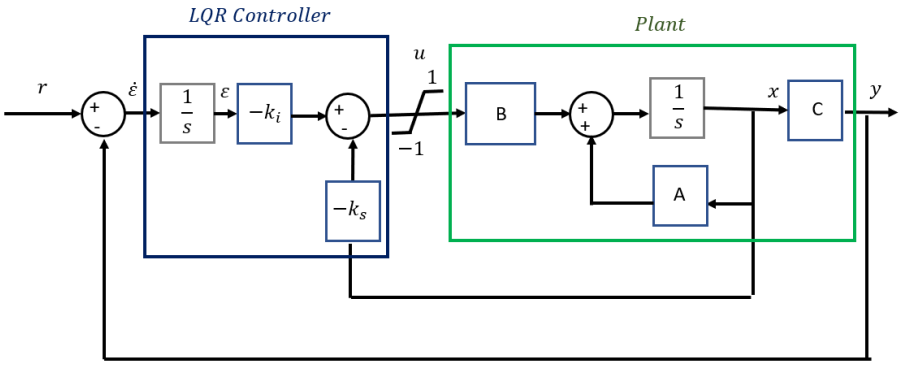

Figure 4.4 Current Control System

The state space representation of the system implemented in the plant is expressed in equation (4.13). The output values described in the figure above, y, is the current connected to the microgrid, i_{2d} and i_{2q}.

This section focuses on the procedure of designing the robust LQR controller for the current flowing through the microgrid. Variable r in Figure 4.4a is the reference current in the dq frame. In the previous chapter the parameters for the LCL filter are designed therefore the plant is known. Reference [40] conducted a similar approach to the LQR control design except that the author considers the parameters to be uncertain. It is verified that the plant is completely state controllable. The transfer function of the plant is

$$G_p(s) = C(sI - A)^{-1}B \tag{4.41}$$

The reference input begins at $t = 0$ and so the state error equation for $\dot{\varepsilon}$ can be incorporated in the LQR design. See [16] for further explanation on deviation of combining both equations within the state space representation which is given by

$$\dot{e}(t) = \begin{bmatrix} \dot{x}_e(t) \\ \dot{\varepsilon}_e(t) \end{bmatrix} = \begin{bmatrix} A & 0 \\ -C & 0 \end{bmatrix} \begin{bmatrix} x_e(t) \\ \varepsilon_e(t) \end{bmatrix} + \begin{bmatrix} B \\ 0 \end{bmatrix} u_e(t) \tag{4.42a}$$

The new equation becomes

$$\dot{e} = \hat{A}e + \hat{B}u_e \tag{4.42b}$$

where

$$\hat{A} = \begin{bmatrix} A & 0 \\ -C & 0 \end{bmatrix} \tag{4.42c}$$

The new input becomes

$$u_e = -\hat{K}e \tag{4.42d}$$

The new gain is defined as

$$\hat{K} = [k_s \quad k_i] \tag{4.42e}$$

where

$$k_s = \begin{bmatrix} k_{11} & k_{12} & \cdots & k_{1n-2} \\ k_{21} & k_{22} & \cdots & k_{2n-2} \end{bmatrix} \tag{4.42f}$$

$$k_i = \begin{bmatrix} k_{1n-1} & k_{1n} \\ k_{2n-1} & k_{2n} \end{bmatrix} \tag{4.42g}$$

Incorporating the new state feedback gain and the integral gain constant in the state error equation can be obtained as

$$\dot{e} = (\hat{A} + \hat{B}\hat{K})e \tag{4.42h}$$

The LQR problem procedure is as follows. There exists a positive semi-definite solution $\bar{P}$ to the algebraic Riccati equation (ARE) as described in chapter 2

$$0 = A^T P + PA - PBR^{-1}B^T P + Q \tag{4.43a}$$

The optimal control state feedback gain is given by

$$u^*(t) = -R^{-1}B^T \bar{P}x(t) \tag{4.43b}$$

Reference [41] provides a proof which states that $u^*(t)$ minimizes the performance index shown in equation (4.43c).

$$J = \int_0^\infty [x(\tau)^T Q(\tau)x(\tau) + u(\tau)^T R(\tau)u(\tau)]d\tau \tag{4.43c}$$

Matrices Q and R within the quadratic cost function are the state and control penalty matrix, respectively. $x(\tau)^T Q(\tau)x(\tau)$ is related to the control accuracy and $u(\tau)^T R(\tau)u(\tau)$ measures the control expenditure [42]. To increase the response time of a state increase q_{nn} so that state will be more penalized. If the cost of the controller is low, then decrease r_{nn} vice versa if the cost of the controller is high.

$$Q = \begin{bmatrix} q_{11} & 0 & 0 & 0 \\ 0 & q_{22} & 0 & 0 \\ 0 & 0 & \ddots & 0 \\ 0 & 0 & 0 & q_{nn} \end{bmatrix} \quad R = \begin{bmatrix} r_{11} & 0 & 0 & 0 \\ 0 & r_{22} & 0 & 0 \\ 0 & 0 & \ddots & 0 \\ 0 & 0 & 0 & r_{nn} \end{bmatrix}$$

The initial terms for q_{nn} and r_{nn} are considered from Bryson's rule [16]

$$q_{nn} = \frac{q_n}{x_n^2} \qquad r_{nn} = \frac{r_n}{u_1^2}$$

The initial penalty is the following

$$Q = \begin{bmatrix} \frac{q_1}{x_1^2} & 0 & 0 & 0 \\ 0 & \frac{q_2}{x_2^2} & 0 & 0 \\ 0 & 0 & \ddots & 0 \\ 0 & 0 & 0 & \frac{q_n}{x_n^2} \end{bmatrix} \quad R = \begin{bmatrix} \frac{r}{u_1^2} & 0 & 0 & 0 \\ 0 & \frac{r_2}{u_2^2} & 0 & 0 \\ 0 & 0 & \ddots & 0 \\ 0 & 0 & 0 & \frac{r_n}{u_n^2} \end{bmatrix} \tag{4.44}$$

Depending on the importance of each state the tuning of q_{nn} and r_{nn} will be conducted accordingly. The state variables used for the LQR design are given as

$$x(t) = [i_{1d}(t) \quad i_{1q}(t) \quad i_{2d}(t) \quad i_{2q}(t) \quad V_{f,d}(t) \quad V_{f,q}(t) \quad e_d(t) \quad e_q(t)]^T \tag{4.45}$$

where $e_d(t)$ and $e_q(t)$ are the error states for the output currents connected to the rest of the microgrid. To obtain an initial value upper bound for the state, the steady-state values are computed by solving for the following equations

$$\begin{cases} 0 = \frac{1}{L_{tot}}(v_{f,d} + R_f i_{1,d} - (R_{tot} + R_f) i_{2,d} + \omega L_{tot} i_{2,q} - v_{g,d}) \\ 0 = \frac{1}{L_{tot}}(v_{f,q} + R_f i_{1,q} - (R_{tot} + R_f) i_{2,q} - \omega L_{tot} i_{2,d} - v_{g,q}) \\ 0 = \frac{1}{L_1}(v_d - (R_1 + R_f) i_{1,d} + \omega L_{1,q} - v_{f,d}) \\ 0 = \frac{1}{L_1}(v_q - (R_1 + R_f) i_{1,q} - \omega L_{1,d} - v_{f,q}) \\ 0 = \frac{1}{C_f}[I_{1d} - I_{2d} + \omega C_f V_{f,q}] \\ 0 = \frac{1}{C_f}[I_{1q} - I_{2q} - \omega C_f V_{f,d}] \end{cases} \tag{4.46}$$

The reference values used after computing the equations from equation (4.46) are

$$Q = \begin{bmatrix} \frac{q_1}{(i_{1dref})^2} & 0 & 0 & 0 & 0 & 0 & 0 & 0 \\ 0 & \frac{q_1}{(i_{1qref})^2} & 0 & 0 & 0 & 0 & 0 & 0 \\ 0 & 0 & \frac{q_2}{(i_{2dref})^2} & 0 & 0 & 0 & 0 & 0 \\ 0 & 0 & 0 & 0.1 & 0 & 0 & 0 & 0 \\ 0 & 0 & 0 & 0 & \frac{q_2}{(v_{fdref})^2} & 0 & 0 & 0 \\ 0 & 0 & 0 & 0 & 0 & \frac{q_2}{(v_{fqref})^2} & 0 & 0 \\ 0 & 0 & 0 & 0 & 0 & 0 & 0.1 & 0 \\ 0 & 0 & 0 & 0 & 0 & 0 & 0 & 0.1 \end{bmatrix}$$

The upper bound constraints for the i_{2qref} are softened because the steady state value was very close to zero and the result in MATLAB returned a floating- point value.

After tuning the Q and R penalty matrices the values are:

$$Q = \begin{bmatrix} 8.539e-07 & 0 & 0 & 0 & 0 & 0 & 0 & 0 \\ 0 & 5.18e-06 & 0 & 0 & 0 & 0 & 0 & 0 \\ 0 & 0 & 8.573e-06 & 0 & 0 & 0 & 0 & 0 \\ 0 & 0 & 0 & 0.1 & 0 & 0 & 0 & 0 \\ 0 & 0 & 0 & 0 & 1.049e-06 & 0 & 0 & 0 \\ 0 & 0 & 0 & 0 & 0 & 0.04351 & 0 & 0 \\ 0 & 0 & 0 & 0 & 0 & 0 & 0.0001479 & 0 \\ 0 & 0 & 0 & 0 & 0 & 0 & 0 & 0.1 \end{bmatrix}$$

$$R = \begin{bmatrix} 1 & 0 \\ 0 & 1 \end{bmatrix}$$

After solving the Riccati equations, the state feedback gain values are the following.

$$k_s = \begin{bmatrix} 0.001097 & -3.304e^{-05} & -5.184e^{-07} & 1.901e^{-07} & 0.003579 & -0.00105 \\ -30304e^{-05} & 0.01131 & -1.225e^{-06} & 0.007842 & -0.002072 & 0.6765 \end{bmatrix}$$

After multiplying the values of the state feedback with the corresponding state variables the optimal system response is achieved regarding overshoot and settling time. After computing the LQR optimization the gain matrix for the PI controller are the following values.

$$k_i = \begin{bmatrix} -0.01216 & -7.34e^{-05} \\ 8.92e^{-06} & -0.1 \end{bmatrix}$$

4.4a Simulation during Steady State

The block diagram from Figure 4.4 is executed in MATLAB/Simulink in Figure 4.5 using steady state values calculated from equations (4.6).

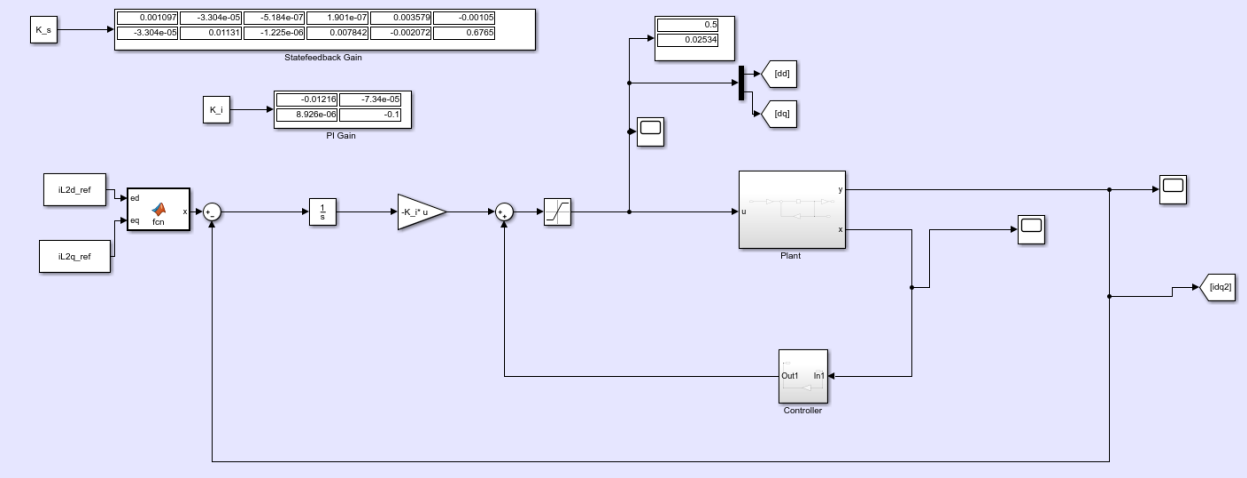

Figure 4.5 Current Controller implemented in SIMULINK

The plant model in Figure 4.5 is expanded in Figure 4.6. The state space representation used is from equation (4.2). Variable x represents the states and y is the output current that is connected to the network.

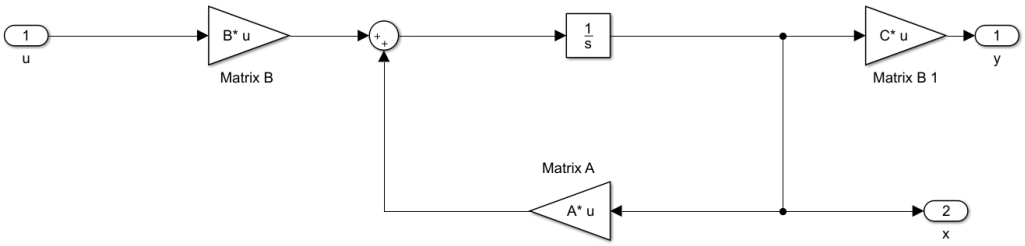

Figure 4.6 Plant Model

The output steady state D axis current reference i_{d2} is 1080A and the output current in the q axis i_{q2} is 0. After using the LQR controller the results in study steady for the current are shown in Figure 4.7

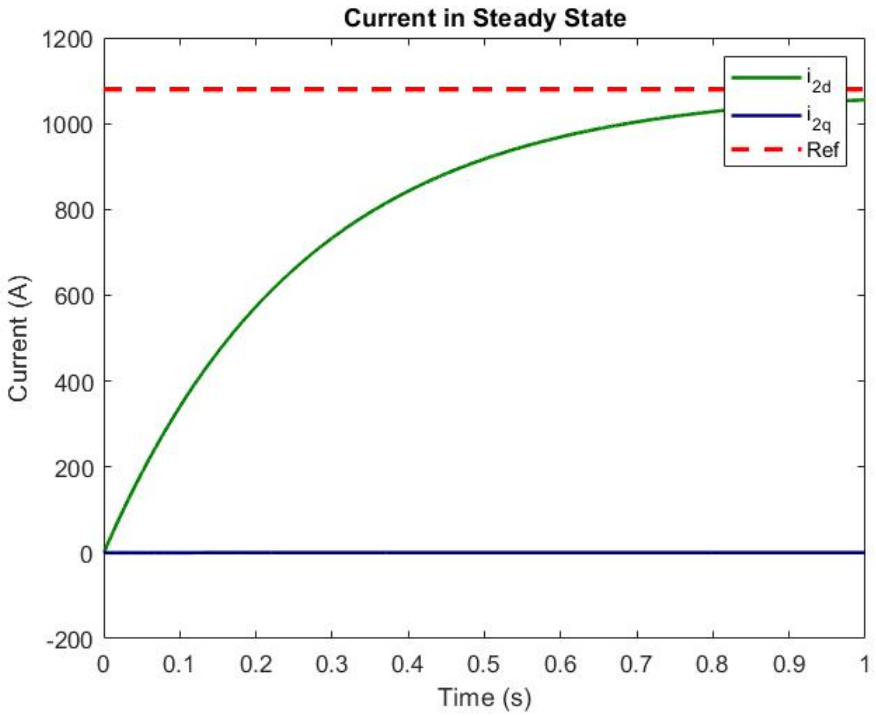

Figure 4.7 Output Current in the DQ frame

The duty cycle is multiplied by the DC component to get the average output variable which in this case is the current. Overall, the duty cycle will influence the output voltage and current. The value of D_d and D_q corresponds to the duty cycle in the dq domain, Figure 4.8 demonstrates the duty cycle during the simulation.

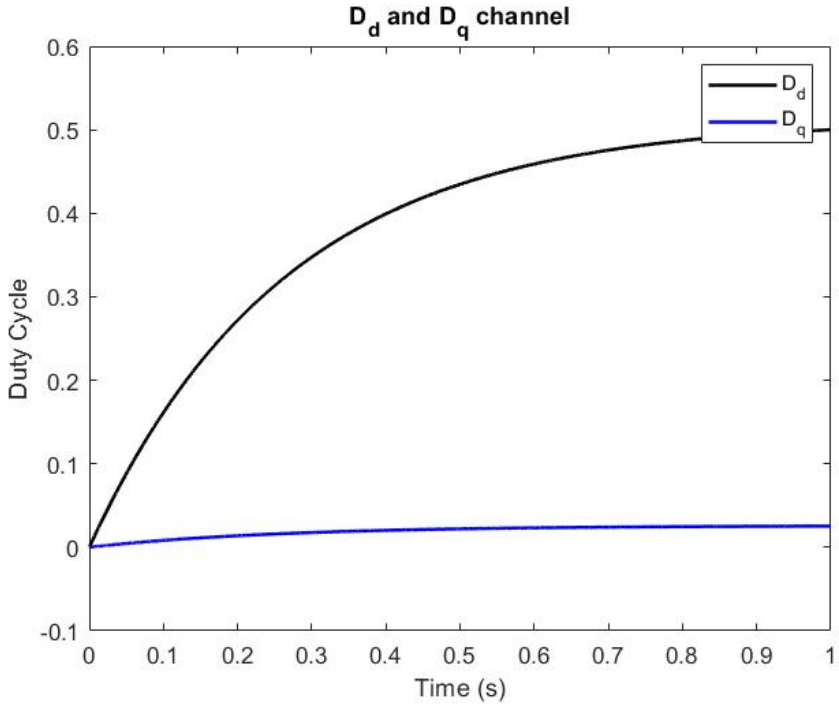

Figure 4.8 Duty Cycle in the DQ frame

4.5 Simulink Implementation

The PI controller is tuned experimentally in MATLAB to receive appropriate gain and phase margins for a stable system. Since the concern is to pick up critical load, the reference of v_q is 0. Similar to the current controller the objective of the voltage controller is to regulate the voltage at the PCC. The phase to phase voltage at the PCC is 480V in the abc-frame and when it is converted to the dq-frame the new value is the following.

$$v_{dq_{LL}} = 480 \times \sqrt{\frac{3}{2}} \tag{4.5a}$$

$$v_{dq_{ph}} = v_{dq_{LL}} \times \frac{1}{\sqrt{3}} \tag{4.5b}$$

$$v_{dq_{peak}} = v_{dq_{ph}} \times \sqrt{2} \tag{4.5c}$$

The peak dq-transformation value of the PCC is 480 V according to equations (4.5a-4.5c). The overall system is depicted in Figure 4.9, the battery storage and diesel generator used to sustain the MG. The PV arrays are ignored in this case study due to the greater influence the battery storage has because of its capacity to pick up load. The dynamics of the battery storage inverter is studied mainly because during the restoration mode the battery storage can pick up the critical load faster than the generator.

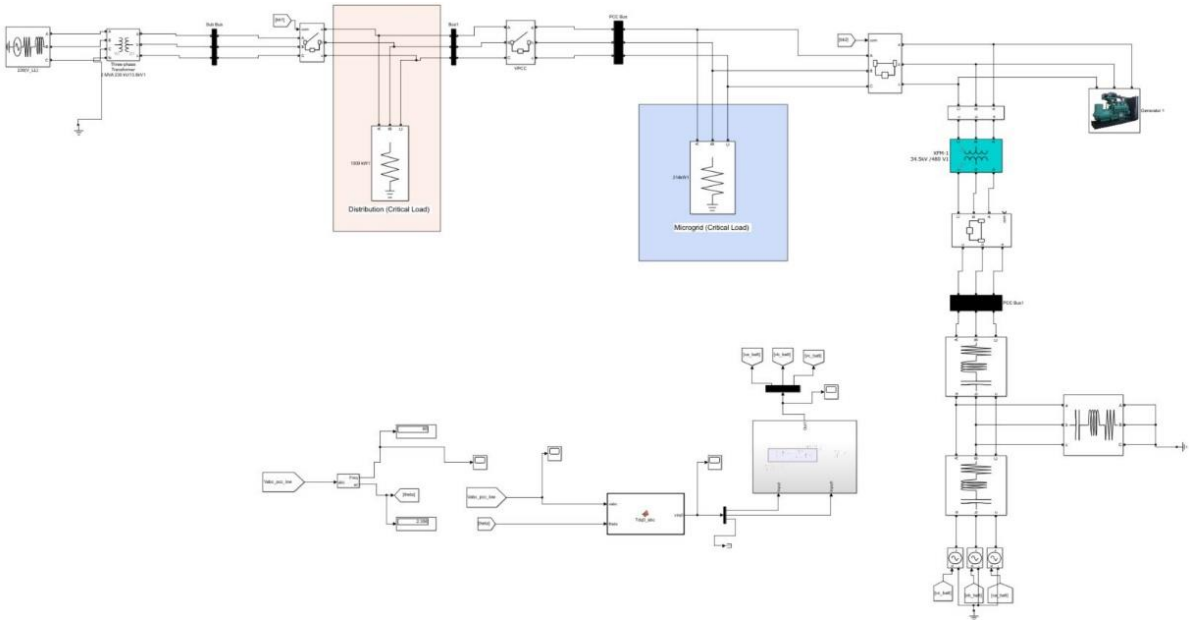

Figure 4.9 SIMULINK Model

Once the load is picked up within the MG the battery will pick up the distribution load at 0.4s.

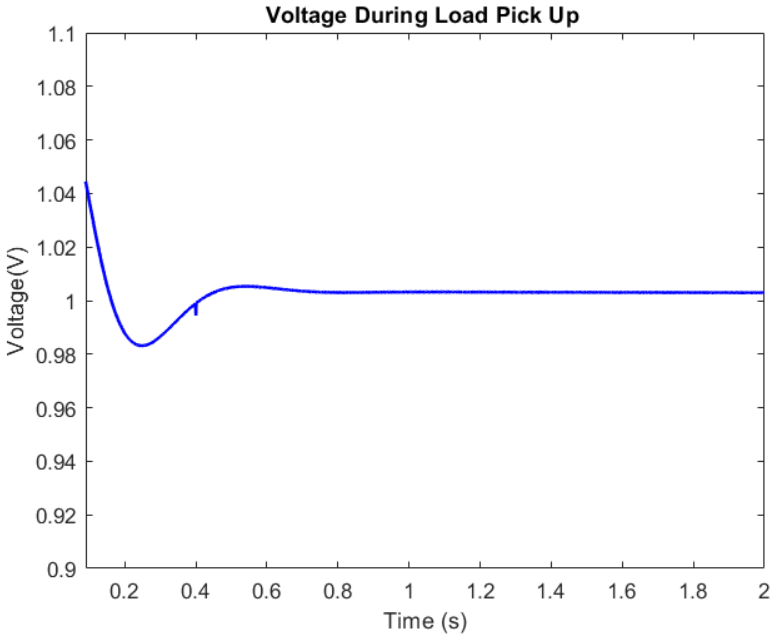

Figure 4.10 Voltage at PCC

The microgrid picks up 100kW from the distribution system. The critical load within the microgrid is the same as the distribution office load assumption made in chapter 3. During load pick at 0.4s, as per Figure 4.12, the voltage is lowered but overall it remains within the IEEE standard 1547 limits.

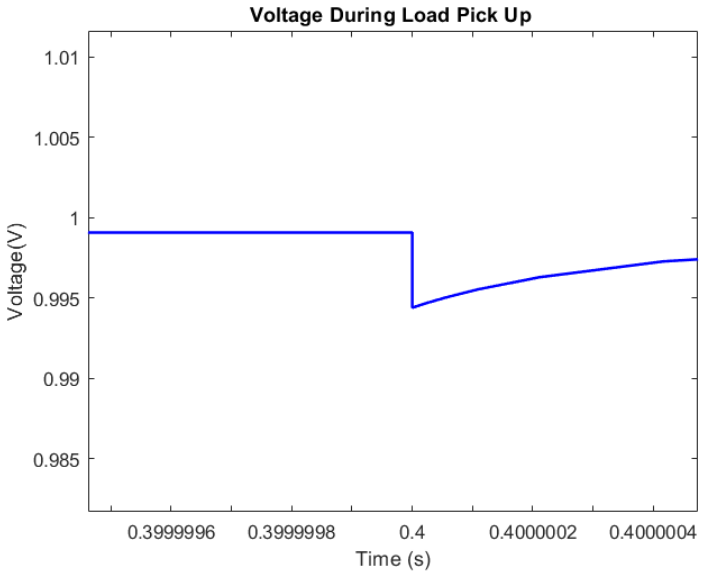

Figure 4.12 Load Pick up Voltage

Previously, in section 4.4 the current did not have an overshoot and the settling time was acceptable. While picking up load the current remained stable as shown in Figure 4.13, this confirms that the current controller is working properly.

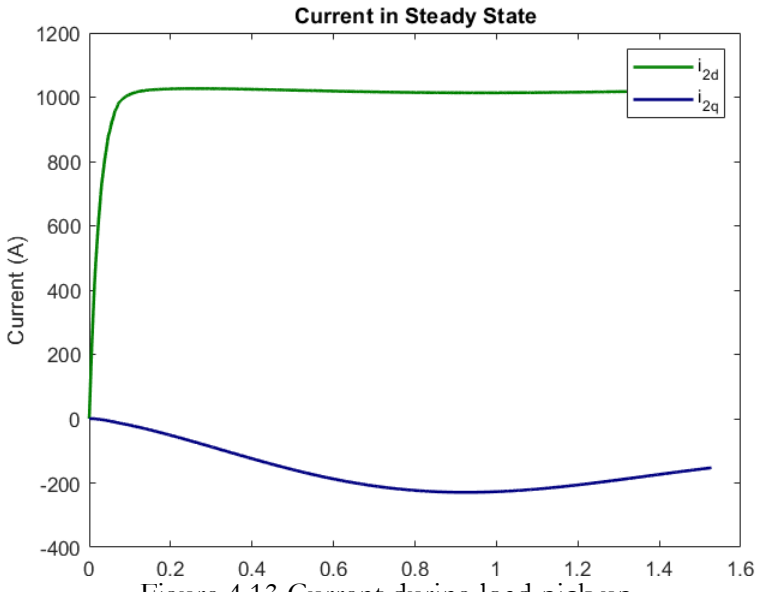

Figure 4.13 Current during load pick up

Chapter 5

Volt/Var Optimization by Inverters and Capacitor Banks

The high penetration of power electronic based distributed energy resources (DERs) has increased the importance and attention given to voltage security of distribution systems. Voltage control in the electrical power system is critical for a proper operating condition and during power restoration voltage [42]. Therefore, distribution systems must have the ability to maintain a secure voltage profile. Using inverters for Volt/VAR control (VVC) can provide a faster response for voltage regulation than traditional voltage regulation devices, such as transformer load tap changers and voltage regulators. The MG designed in chapter 3 can be coupled to aid the voltage regulation when it's integrated into a distribution model with the appropriate voltage level.

5.1 Introduction

The increase of power electronic based DER interconnections on the distribution system has shown the ability to impact voltage regulation and performance. Traditionally, VVC is conducted by transformer load tap changers, voltage regulators, and capacitor banks. The increase of power electronics in the electric power system (EPS) has increased the level of interest to other VVC methods, e.g., STATCOM and the inverters that interface photovoltaics (PVs) and battery energy storage system (BESS) to the grid. As power electronic technology advances, smart solar inverters now have the capability to stay connected to the grid during small disturbances rather than disconnecting from the grid. As per the new IEEE 1547 standard, distributed generation that is inverter-based is required to stay connected to the grid during voltage and frequency ride through [5]. Inverter controls have been designed to inject/absorb reactive power based on the deviations in voltage magnitude.

Power system operators maintain power system security, reduce power losses and the generation cost by utilizing the optimal power flow (OPF) analysis to operate the transmission system [42]. Power flow analysis and modelling is analysed in [43]-[46]. The branch flow model with two relaxation steps analyzes the optimal power flow (OPF) for radial and meshed networks [38]. Since most distribution circuits are radial networks, reference [44] proposes a robust method to solve the distribution system power flow for a radial feeder. The phase angles of the currents and voltages are omitted. A nonlinear model generally has a high computational cost. If the power losses are ignored in the power flow model, a linearized distribution flow model (LinDistFlow) is obtained [45]. A linearized model leads to a convex optimization problem. However, a linearized model incorporating capacitor banks has not been considered.

Reference [46] proposes a technique for volt/var optimization incorporating the interaction between inverters and capacitors using conditional-value-at-risk to obtain a convex approximation. In reference [47], an algorithm is designed to minimize losses and flatten the voltage profile. Reference [48] obtains the reactive injection values of the inverters using nonlinear control policies determined by kernel-based learning. In this case, the communication overhead is reduced to a 30-min basis. To coordinate existing VVC devices and inverters, reference [49] proposed a hybrid VVC scheme.

This paper proposes a technique to determine the optimal reactive power injection or absorption needed from either the inverter or capacitor bank to minimize voltage deviations using mixed integer quadratic programming. Gurobi/MATLAB is used to implement the algorithm that optimizes the reactive power injection or absorption when there is a load pick up during restoration or load shedding when there is an insufficient power supply. A case study based on a 13-node distribution system is presented with DERs connected to multiple buses and two capacitor banks connected to the node. This algorithm is implemented in an environment of centralized dispatch. This paper proposes a mixed-integer quadratic programming problem that is solved using the Big-M method and obtains the global solution.

The continuation of the paper is organized as follows. Section II formulates the problem statement that is being addressed. Section III describes the optimization method used to determine the reactive power injection. Section IV describes the 13-node feeder model and the two simulation cases that are conducted. Section V provides the conclusion and future extension of this work.

5.2 Problem Formulation

The two objectives of this research are to minimize the voltage deviations from the nominal value by controlling reactive power injections from inverters and, if there is a capacitor bank connected to a node, to determine whether to turn on or off the capacitor bank. The proposed Volt/VAR optimization method is based on the approximate linearized distribution flow (LDF) model (1a) proposed in [50]. This method is adopted for this project due to its high computational performance. The radial single-phase distribution system has N+1 node. N_0 corresponds to the substation node, as seen in Figure 1. The voltage at the substation node is the nominal voltage. $v_0 1_N$ denotes the nominal squared voltages. Variable v_n represents the squared voltage magnitude of the nodes n, excluding the substation node.

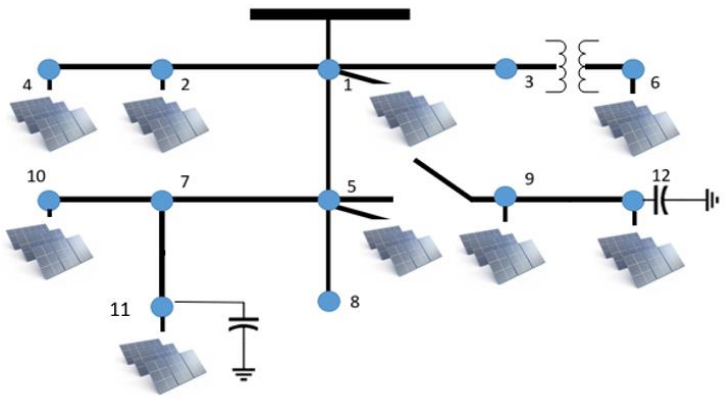

Figure 5.1 IEEE 13 Node Distribution System

DERs are placed at every nonzero node in the network according to the IEEE 13 node test feeder. The active and reactive power are generated by the DERs connected to the grid at node n = {1, ..., N}, represented by $(p_g^n, q_g^n)_{n=1}^N$. $(p_c^n, q_c^n)_{\mathrm{n=1}}^{\mathrm{N}}$ is the power consumed by the load at node n. It is assumed that p_g, p_c and q_c are known quantities.

The active and reactive power injections are:

$$p = p_g - p_c$$
$$q = q_g - q_c$$

Matrix A is the reduced branch-bus incidence matrix of the distribution system. The resistance and reactance of the lines in vector r and x are given based on the IEEE 13 node test feeder configuration impedance. z = r+jx and Z =diag(z), when equation (5.1a) is multiped by A^{-1} and then S =$A^{-T}s$ is substituted. Using the property $A^{-1}\ a_0 = -1_N$ will simplify the equation to (1b). R and X are symmetric positive definite matrix and are expressed in (1c-1d); see [48] for a similar linear approximation model.

$$Av = 2Re[Z^*S] - a_0 v_0 \quad (5.1a)$$

$$v_n \simeq Rp + Xq + v_0 1_N \quad (5.1b)$$

$$X = 2A^{-1}diag(x)A^{-T} \quad (5.1c)$$

$$R = 2A^{-1}diag(r)A^{-T} \quad (5.1d)$$

When the active and reactive power injections, p and q, are given, the voltage deviation can be found by a linear equation as per [51]

$$\Delta v \simeq Rp + Xq \quad (5.1d)$$

$$\Delta v = \begin{bmatrix} v_1 - v_0 \\ \vdots \\ v_N - v_0 \end{bmatrix}$$

where $Rp + Xq$ demonstrates the voltage drop in the line due to the line impedance. Where Δv represents the deviation in squared voltages. When the reactive power injection of the capacitor bank is incorporated, the new linearized distribution flow model is given by:

$$\Delta v \simeq R(p_g - p_c) + X((q_g - q_c) + q_{cb}) \quad (5.2a)$$

The following values are given as measurements:

p_g: Active solar generation
p_c: Active load consumed
q_c: Reactive load consumed

There are two optimization variables:

q_{cb}: Reactive power produced by the capacitor banks
q_g: Reactive solar generation

The objective is to minimize the voltage deviations by minimizing the l_2-norm of vector Δv.

$$\min\|\Delta v\|_2^2 \tag{5.2b}$$

Based on the apparent power capacity of the inverters and the constraint not to create reverse power flow, the following constraints are enforced. The limits are given:

$$p_g^2 + q_g^2 \leq \left(S_g^{max}\right)^2 \tag{5.3}$$

IEEE 1547 standard [1] states that voltage distortion limits for a node voltage at the point of common coupling (PCC) should be 3% for any voltage that is 69 kV or below. dv_n is the absolute deviation voltage. Hence,

$$dv_n^{min} \leq dv_n \leq dv_n^{max} \quad \forall n \tag{5.4a}$$

$$-0.03 \leq dv_n \leq 0.03 \tag{5.4b}$$

Given the constraints and objective function, the computational problem can be solved by mixed integer quadratic programming. There are switched capacitor banks within the network. When the capacitor bank is switched on it injects reactive power to the bus and when it is off it does not. Let x_s be a binary variable that is used to indicate if the capacitor bank is switched on or off. Equation (5.5) expresses what the value of q_{cb} will be depending on whether x_s is 0 or 1. ω is the angular velocity at 60Hz and v_{cb} is the voltage of the node connected to the capacitor bank.

$$q_{cb} = \begin{cases} v_{cb}\omega C, & x_s = 1 \\ 0, & x_s = 0 \end{cases} \tag{5.5}$$

v_{cb} is an unknown variable and $\mathrm{x_s}$ is an unknown binary variable. The value of $\mathrm{q_{cb}}$ is given by

$$q_{cb} = v_{cb}\omega C x_s \tag{6a}$$

Note that q_{cb} is a nonlinear equation. A technique used to linearize equation (5.6a) is the Big-M method which introduces different inequalities and the large positive number M. Consider the constraint $q_{cb} = v_{cb}\omega\mathrm{C}\mathrm{x_s}$, if $v_{cb}\omega\mathrm{C}$ is bounded with $v_{cb}\omega\mathrm{C} \in [-\mathrm{M}, \mathrm{M}]$, the new constraints can also be expressed as

$$-Mx_s \leq q_{cb} \leq x_s M \tag{5.6b}$$

$$-M(1 - x_s) \leq q_{cb} - v_{cb}\omega C \leq (1 - x_s)M \tag{5.6c}$$

$$x_s \in \{0,1\} \tag{5.6d}$$

If $x_s = 1$, then constraint (5.6c) becomes an equality and q_{cb} is less than the upper bound M, due to constraint (5.6b). When $x_s = 0$ then the first inequality (5.6b) ensures $q_{cb} = 0$. Minimizing the voltage deviations can be solved using the gurobi solver in MATLAB by conducting mixed integer quadratic programming computation.

5.3 Numerical Tests

According to the IEEE 13-node test feeder, nodes 3, 7, and 8 do not have any load connected to it as shown in Figure 1. In this system, the capacitor bank injection at node 11 is 100 kVAR and 200 kVAR at node 12, respectively. In this distribution model, aluminium conductors steel-reinforced (ACSR) of the aluminium area 556,500 26/7 cmil is used. The real data used in this case study was taken from the Pecan St dataset [52]. The minute-sampled PV generation and loads data is taken on May 1, 2013, at 8:00 am. The load was scaled so that the monthly peak will be equivalent to 30% of the benchmark load values. A random lagging power factor between 0.85 to 0.9 is used to generate the reactive loads.

5.4 Simulation Cases

Since diverse loads have been added to the EPS and load forecast is difficult, it is desirable to have a continuous device that regulates the voltage profile. The penetration of inverter based DERs is increased in the distribution system and, therefore, using the inverters for voltage regulation is a feasible solution. Switched capacitor banks are already integrated within the distribution system and so enabling these two devices to work together is the objective of this study. In this simulation case, the load demand of the customer is increased, and it is intended to evaluate how the inverter and capacitor bank in the system can help eliminate the voltage deviations. The results are analysed while there is a decrease in load to observe how the inverter and capacitor bank will react and whether the voltages will stay within its constraints. If either one of the two scenarios occur, there can be an imbalance in power generation, leading to under-frequency, angle instability, voltage violations, and overloading other generation units in the power system.

5.4.1 Simulation Case 1

Both simulation cases use a 13-node radial test feeder with DERs connected to 9 out of the 12 nodes. It is not practical to expect a DER at every node of the distribution system. Other techniques such as LTC or a capacitor bank are used to regulate the voltage. This simulation case is developed to observe if the capacitor bank should be switched on or off, depending on the amount of reactive power that is needed for voltage regulation. The initial voltage and reactive power are shown in Figure (5.2a-5.2b).

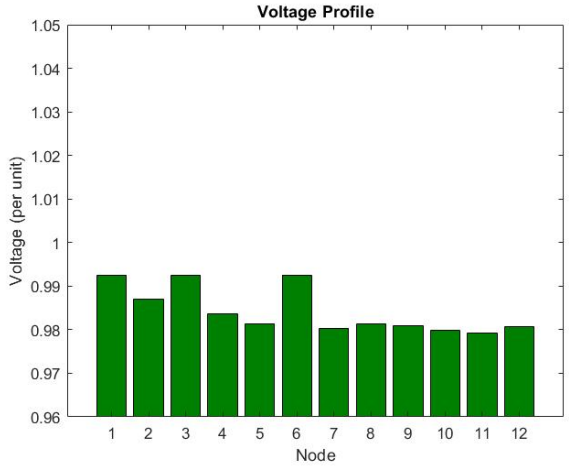

Figure 5.2a Voltage at each node

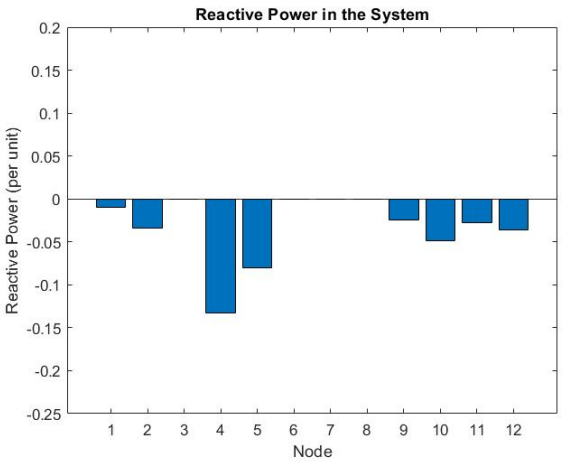

Figure 5.2b Reactive power at each node

Case 1 represents what may occur when there is a high customer demand. As the power consumption increases, low voltage violations occur as illustrated by Figure (5.3a). The power consumed in the entire system is increased by 50%, causing a voltage dip. When using the controller, the voltage remains within tolerance as shown in Figure (5.3b).

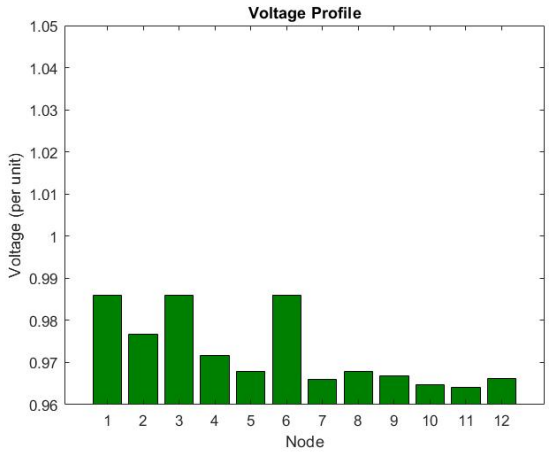

Figure 5.3a Voltage of profile without controller implemented during load increase

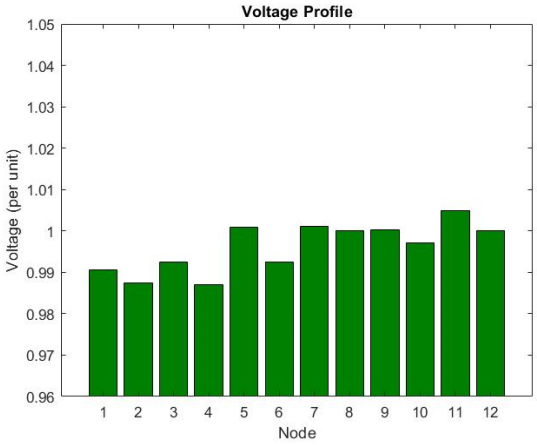

Figure 5.3b Voltage of profile with controller implemented during load increase

Figure (5.4a-5.4b) demonstrates the output reactive power of the DER inverters and capacitor bank at its corresponding node. The active power generated is kept constant according to the measured value at that time. Figure 5.4a occurs when no controller is implemented. Figure 5.4b includes control, when the power consumption increases the amount of reactive power absorption decreases to mitigate the voltage deviations. The capacitor bank at node 11 is switched on because the closest inverter has reached the maximum level of reactive power output capacity.

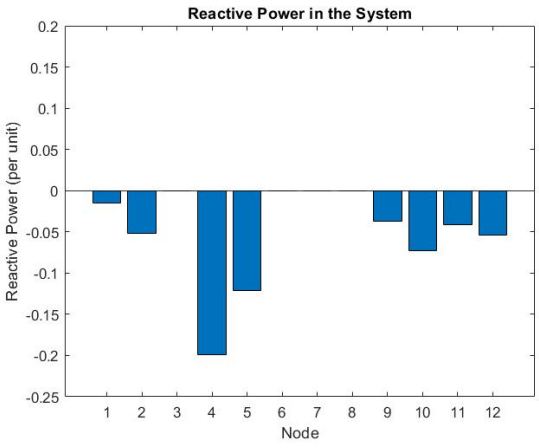

Figure 5.4a Reactive power at each node during load increasing without a controller

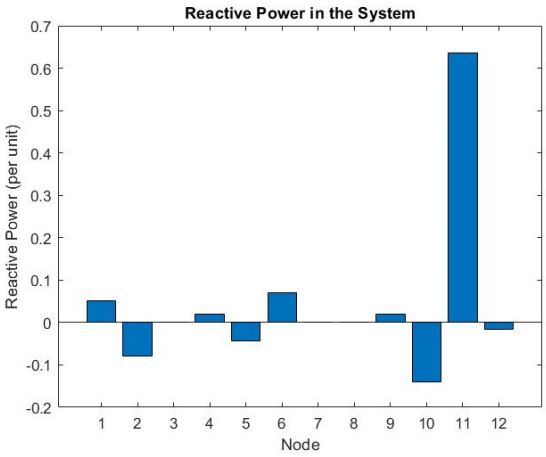

Figure 5.4b Reactive power at each node during load increasing with a controller

5.4.2 Simulation Case 2

In the second case the active power consumed in the entire system is decreased by 50% and the reactive power consumed is calculated based on the randomized power factor. Like the first simulation

case, the voltage profile is depicted in Figure (5.5a-5.5b). For the case with control the voltage has a maximum of 0.5% error.

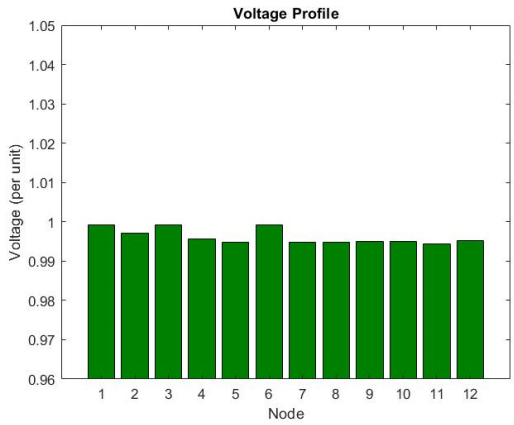

Figure 5.5a Voltage profile during load decrease with no controller

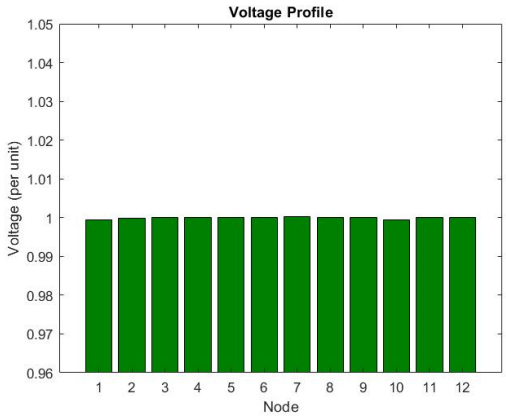

Figure 5.5b Voltage profile during load decrease with a controller

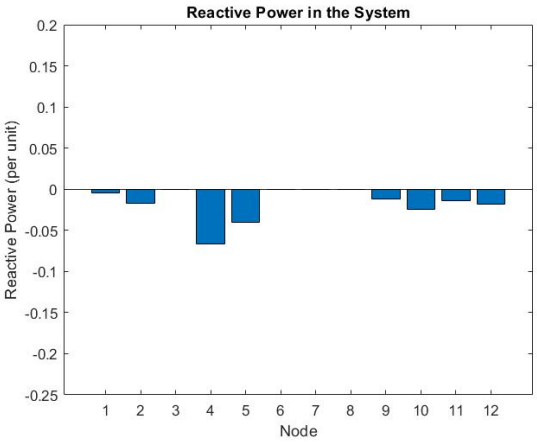

Figure 5.6a Reactive power at each node during load decreasing without a controller

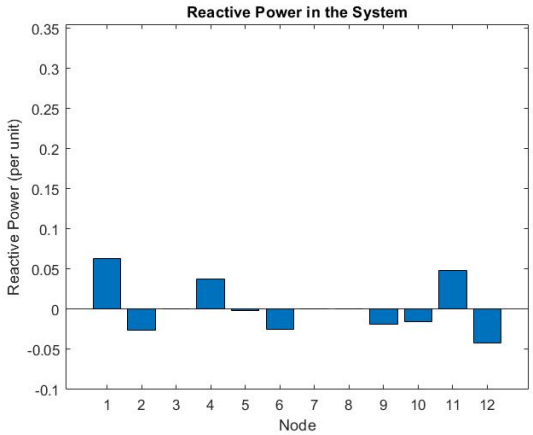

Figure 5.6b Reactive power at each node during load decreasing with a controller

In the second simulation case, the active power generated by the DERs is the same as that in the first simulation case. In case 2 both capacitors are off because there is a rise in voltage, as per Figure (5.5a-5.5b). These results are generated using MATLAB, YALMIP toolbox and the gurobi optimization solver.

5.5 Conclusion

This research formulates the optimization problem to dispatch the reactive power generated by inverters and utilize the mixed integer quadratic programming method to solve this problem It can be used to determine the reactive power inverters can produce to eliminate voltage violations in the distribution system. The simulation cases in this research are used to validate how the proposed method mitigates voltage-dips and voltage swells using inverters and capacitor banks. This work can be used by system operators to schedule proper dispatch and improve power quality. The computational framework can also be used within a centralized control environment to provide the

reactive power references for local controllers within the DER. The proposed computational method is validated by demonstrating how the voltage profile remains within the appropriate tolerance given by standard 1547 [5]. VVC for a single-phase distribution system that contains DER at multiple nodes has been included in this research. Although the fixed capacitor bank included in the system is economical, its rigid reactive power supply is not ideal for a dynamic system. An automatic capacitor bank can keep a constant high-power factor under fluctuating loads. A limitation of this work is that it does not evaluate the behavior of other VVC devices such as transformer load tap changer and voltage regulators. This model also ignores the power losses. The future work can include the application of the proposed method to the Dominion Energy system. Also, instead of the LinDistFlow model, a linear approximation of the multiphase branch model will be studied. This model can be applied to an unbalanced three phase system.

Chapter 6

Summary and Future work

To conclude, the objective of this thesis is to explore the possibilities of improving power quality and picking up critical load using an inverter-based DER and MGs. A computationally framework has been developed to dispatch the reactive power generated by inverters by using a mixed integer quadratic programming method. It can be used to determine the reactive power inverters can produce to eliminate voltage violations in the distribution system. A MG based on Dominion Virginia Power campus was designed by conducting load estimation, designing PV generation and battery storage, and constructing a RTDS model to run simulations on different case studies. The two case studies included were the synchronization of the MG to the grid and using battery storage to support frequency regulation. Finally, the focus is to develop a current and voltage controller during load pick up for the battery storage system. The controllers performed as expected to improve the power quality of the network. The future work consists of:

- Include droop control for frequency and voltage regulation by generating the droop slope for the inverter.
- Creating a model of the MG in PSCAD and interface it with MATLAB to study the transients of the simulation while still incorporating the optimal controller.
- Integrate the Volt/Var computational method to Dominion Energy's system.

Bibliography

[1] Campbell, Alexia Fernández. 2018. "It Took 11 Months to Restore Power to Puerto Rico after Hurricane Maria. A Similar Crisis Could Happen Again." Vox. Vox. August 15, 2018. https://www.vox.com/identities/2018/8/15/17692414/puerto-rico-power-electricity-restored-hurricane-maria.

[2] Ton, Dan T., and Merrill A. Smith. 2012. "The U.S. Department of Energy's Microgrid Initiative." Electricity Journal 25 (8): 84–94.

[3] R. H. Lasseter, "MicroGrids," 2002 IEEE Power Engineering Society Winter Meeting. Conference Proceedings (Cat. No.02CH37309), New York, NY, USA, 2002, pp. 305-308 vol.1.

[4] L. Funicello-Paul, "Navigant Research Identifies 1,869 Microgrid Projects, Representing Nearly 21 GW of Capacity", Navigantresearch.com, 2018. [Online]. Available: https://www.navigantresearch.com/news-and-views/navigant-research-identifies 1869microgrid-projects-representing-nearly-21-gw-of-capacity. [Accessed: 09- June- 2018].

[5] IEEE Standard for Interconnection and Interoperability of Distributed Energy Resources with Associated Electric Power Systems Interfaces," in IEEE Std 1547-2018 (Revision of IEEE Std 1547-2003), vol., no., pp.1-138, 6 April 2018

[6] "Dominion Energy Launches Grid Transformation Program, Paving Way for Virginia's Energy Future With 3,000 Megawatts of New Solar and Wind Planned by 2022", Prnewswire.com, 2018. [Online]. Available: https://www.prnewswire.com/news releases/dominion-energy-launches-grid-transformation-program-paving-way-for- virginias-energy-future-with-3-000-megawatts-of-new-solar-and-wind-planned-by- 2022--300685854.html. [Accessed: 25- Jul- 2018].

[7] M. M. Adibi and R. J. Kafka, "Power System Restoration Issues," in *IEEE Computer Applications in Power*, vol. 4, no. 2, pp. 19-24, April 1991.

[8] F. Katiraei and M. R. Iravani, "Power Management Strategies for a Microgrid With Multiple Distributed Generation Units," in *IEEE Transactions on Power Systems*, vol. 21, no. 4, pp. 1821-1831, Nov. 2006.

[9] Y. Xu, C. Liu, K. P. Schneider, F. K. Tuffner and D. T. Ton, "Microgrids for Service Restoration to Critical Load in a Resilient Distribution System," in *IEEE Transactions on Smart Grid*, vol. 9, no. 1, pp. 426-437, Jan. 2018.

[10] C. L. Moreira, F. O. Resende and J. A. P. Lopes, "Using Low Voltage MicroGrids for Service Restoration," in *IEEE Transactions on Power Systems*, vol. 22, no. 1, pp. 395-403, Feb. 2007.

[11] A. G. Tsikalakis and N. D. Hatziargyriou, "Centralized Control for Optimizing Microgrids Operation," *2011 IEEE Power and Energy Society General Meeting*, Detroit, MI, USA, 2011, pp. 1-8.

[12] C. C. Liu, "Reliable Distribution Systems Are Not Resilient?" "In My View," IEEE Power and Energy Magazine, May/June 2015, pp. 93-96.

[13] H. Gao, Y. Chen, Y. Xu, C. C. Liu, "Resiliency-Oriented Critical Load Restoration Using Microgrids in Distribution Systems," IEEE Trans. Smart Grid, Nov. 2016, pp. 2837 - 2848.

[14] J. Li, X.-Y. Ma, C. C. Liu, K. Schneider, "Distribution System Restoration with Microgrids Using Spanning Tree Search," IEEE Trans. Power Systems, Nov. 2014, pp. 3021-3029.

[15] Yazdani, Amirnaser, and Reza Iravani. Voltage-Sourced Converters in Power Systems: Modeling, Control, and Applications. Wiley, 15 Feb. 2010.

[16] R. H. Park, "Two-reaction Theory of Synchronous Machines Generalized Method of Analysis-Part I," in *Transactions of the American Institute of Electrical Engineers*, vol. 48, no. 3, pp. 716-727, July 1929.

[17] P. Rodriguez, J. Pou, J. Bergas, J. I. Candela, R. P. Burgos and D. Boroyevich, "Decoupled Double Synchronous Reference Frame PLL for Power Converters Control," in *IEEE Transactions on Power Electronics*, vol. 22, no. 2, pp. 584-592, March 2007.

[18] S. Golestan, M. Monfared and F. D. Freijedo, "Design-Oriented Study of Advanced Synchronous Reference Frame Phase-Locked Loops," in *IEEE Transactions on Power Electronics*, vol. 28, no. 2, pp. 765-778, Feb. 2013.

[19] B.D.O.Anderson, J.B.Moore, Optimal Control, Prentice Hall, 1989

[20] K. Ogata Modern Control Engineering. Upper Saddle River, N.J: Prentice Hall, 1997. Print.

[21] P. Dorato, C.T Abdallah, and V. Cerone. Linear Quadratic Control: An Introduction. Krieger Publishing, 1995

[22] J. P. Hespanha (2009). Linear Systems Theory. Princeton Press, Princeton, New Jersey.

[23] G. Alvarez, C. MERTZ, J. PETTI, R. LIU, H. M. CHOU, K. THOMAS "Design and Synchronization of the Dominion Energy Microgrid", 2018 CIGRE US National Committee 2018 Grid of the Future Symposium, Reston, Virginia, 2018

[24] Woolf, H. M. (1968). "On the Computation of Solar Elevation Angles and the Determination of Sunrise and Sunset Times", National Aeronautics and Space Administration report no. NASA TM X-164, September.

[25] C. Landau, "Optimum Tilt of Solar Panels", Solarpaneltilt.com, 2001. [Online]. Available: http://solarpaneltilt.com/#fixed. [Accessed: 09- Jun- 2018]

[26] "UO SRML: Sundial program", Solardata.uoregon.edu, 2018. [Online]. Available: http://solardata.uoregon.edu/SunDialProgram.html. [Accessed: 02- Jun- 2018].

[27] "HelioScope: Advanced Solar Design Software", Helioscope.com, 2018. [Online]. Available: https://www.helioscope.com/. [Accessed: 10- Jun- 2018].

[28] Taheri, Sina & Kekatos, Vassilis & Veeramachaneni, Sriharsha. (2019). Energy Storage Sizing in Presence of Uncertainty.

[29] W. Choi et al., "Reviews on Grid-Connected Inverter, Utility-Scaled Battery Energy Storage System, and Vehicle-to-Grid Application - Challenges and Opportunities," 2017 IEEE Transportation Electrification Conference and Expo (ITEC), Chicago, IL, 2017, pp. 203210.

[30] P. Sharma, "Safety First: Today's Li-ion Batteries in UPSs Are Safe, Long-Lasting, and Less Costly", APC Blog & Community Site, 2018. [Online]. Available: https://blog.apc.com/2018/02/07/safety-li-ion-batteries-ups/. [Accessed: 14- Jun- 2018]

[31] S. Taheri, V. Kekatos and G. Cavraro, "An MILP Approach for Distribution Grid Topology Identification using Inverter Probing," 2019 IEEE Milan PowerTech, Milan, Italy, 2019, pp. 1-6.

[32] M. Masters, Gilbert. (2005). Renewable and Efficient Electric Power Systems

[33] "Real Time Digital Power System Simulator • RTDS Technologies Inc.", RTDS

[34] T. Barik . "Synchrophasor Based Centralized Remote Synchroscope for Power System Restoration." M.S. Thesis, Virginia Polytechnic Institute and State University, USA, 2018

[35] LC filter design for high-power PWM voltage source inverter Spmg Qiang (Dept. of Electr. Eng., Tsinghua Univ., Beijing, China); Liu Wenhua; Yan Gangui; Chen Yuanhua Source: Journal of Tsinghua University (Science and Technology), v 43, n 3, p 345-8, March 2003

[36] A novel filter design for output LC filters of PWM inverters (Open Access)
Kim, Hyosung (School of EE and Control Eng., Kongju National University, Cheonan, Korea, Republic of); Sul, Seung-Ki Source: Journal of Power Electronics, v 11, n 1, p 74-81, January 2011

[37] A. Reznik, M. G. Simões, A. Al-Durra and S. M. Muyeen, "LCL Filter Design and Performance Analysis for Grid-Interconnected Systems," in *IEEE Transactions on Industry Applications*, vol. 50, no. 2, pp. 1225-1232, March-April 2014.

[38] R. Boylestad, and L. Nashelsky. Electronic Devices and Circuit Theory. 11th ed., Pearson Prentice Hall, 2013.

[39] Hiti, Silva. 1995. "Modeling and Control of Three-Phase PWM Converters," July. http://hdl.handle.net/10919/77984.

[40] P. Buduma and G. Panda, "Robust Nested Loop Control Scheme for LCL-Filtered Inverter-Based DG Unit in Grid-Connected and Islanded Modes," in *IET Renewable Power Generation*, vol. 12, no. 11, pp. 1269-1285, 20 8 2018.

[41] Ogata, Katsuhiko. 2009. Modern Control Engineering (5th Edition). 5 editions. Pearson.

[42] M. K. Singh, V. Kekatos, and C.-C. Liu, "Optimal distribution system restoration with microgrids and distributed generators," IEEE Power and Energy Society General Meeting (PES-GM), Atlanta, GA, Aug. 2019.

[42] M. Hadi Amini, S. Bahrami, F. Kamyab, S. Mishra, R. Jaddivada, K. Boroojeni, P. Weng, and Y. Xu, Chapter 6 - Decomposition Methods for Distributed Optimal Power Flow: Panorama and Case Studies of the DC Model, Classical and Recent Aspects of Power System Optimization, Academic Press 2018, pp. 137-155.

[43] M. Farivar and S. Low, 'Branch Flow Model: Relaxations and Convexification – Part I,' IEEE Trans. on Power Systems, Vol. 28, No. 3, Aug. 2013.

[44] M. Baran and F. Wu, 'Optimal Sizing of Capacitors on a Radial Distribution System,' IEEE Trans. on Power Delivery, Vol. 4, No. 1, Jan. 1989.

[45] V. Kekatos, L. Zhang, G. Giannakis and R. Baldick, "Voltage Regulation Algorithms for Multiphase Power Distribution Grids," *2016 IEEE Power and Energy Society General Meeting (PESGM)*, Boston, MA, 2016.

[46] K. S. Ayyagari, N. Gatsis, A. F. Taha, and B. Dong, "On Static and Adaptive Policies for Chance-Constrained Voltage Regulation," *2018 52nd Asilomar Conference on Signals, Systems, and Computers*, Pacific Grove, CA, USA, 2018, pp.

[47] H.-G. Yeh, D. F. Gayme, and S. H. Low, "Adaptive VAR Control for Distribution Circuits with Photovoltaic Generators," IEEE Trans. Power Syst., vol. 27, 2012, pp. 1656–1663.

[48] A. Garg, M. Jalali, V. Kekatos, and N. Gatsis, "Kernel-Based Learning for Smart Inverter Control," 2018 IEEE Global Conference on Signal and Information Processing (GlobalSIP), Anaheim, CA, USA, 2018, pp. 875-879

[49] Z. Wang, H. Chen, J. Wang, and M. Begovic, "Inverter-less Hybrid Voltage/Var Control for Distribution Circuits with Photovoltaic Generators," in *IEEE Transactions on Smart Grid*, vol. 5, no. 6, Nov. 2014, pp. 2718-2728.

[50] V. Kekatos, L. Zhang, G. B. Giannakis, and R. Baldick, "Fast Localized Voltage Regulation in Single-Phase Distribution Grids," 2015 IEEE International Conference on Smart Grid Communications (SmartGridComm), Miami, FL, 2015, pp. 725-730.

[51] M. Farivar, L. Chen, and S. Low, "Equilibrium and Dynamics of Local Voltage Control in Distribution Systems," 52nd IEEE Conference on Decision and Control, Florence, 2013, pp. 4329-4334.

[52] (2018) Pecan Street Inc. Dataport. [Online]. Available: https: //dataport.cloud/